Facultad de Física

Pontificia Universidad Católica de Chile

Master's Thesis submitted to Physics Faculty at
Pontificia Universidad Católica de Chile, Santiago, Chile
for the degree of
Master of Science

submitted by
Daniela Alejandra, Díaz Contreras

born in Santiago, Chile
2018

Medical Faculty Heidelberg

Ruprecht-Karls-University Heidelberg

Master's Thesis

"Clinical Medical Physics"

submitted by

Daniela Alejandra, Díaz Contreras

born in Santiago, Chile

2018

Characterization of the ionizing radiation emission

of a plasma focus device

This Master's thesis has been composed by Daniela A., Díaz Contreras

at Pontificia Universidad Católica de Chile

under the supervision of

Prof. Paola Caprile, PhD.

Pontificia Universidad Católica de Chile

and

Prof. José A. Moreno, PhD.

Comisión Chilena de Energía Nuclear (CCHEN)

and

Prof. Andrea Schwahofer, PhD.

Heidelberg University

Abstract

The PF2kJ plasma focus device was studied as a pulsed source of x-rays neutron radiation. X-rays are emitted during the focalization process of the plasma if the device is operated using hydrogen as the filling gas. Fusion reactions can be obtained if deuterium gas is used, with the consequent emission of fast neutrons. The x-ray emission is characterized by spatial distribution measurements by using TLD100 dosimeters and radiochromic films, the linearity of the output, as well as the effective energy of the x-ray radiation by measuring transmission through different aluminum thicknesses. A low effective energy of 7.5 keV is estimated. The variation of the intensity of the emission in distance and the assessment of the radiation levels which a device operator may be exposed are also included as part of the x-ray emission characterization study. Personal equivalent dose value of 2.8 mSv/year is estimated in a normal regime of the device operation. This level is not harmful based on ICRP recommendations.

Fast neutron fluence of the order of 10^5 n/cm^2 per shot in 4π sr is estimated by means of ^{3}He proportional detector, and preliminary measurements are performed by using pairs of TLD 600 and TLD 700 dosimeters.

Declaration:

I hereby certify, that I have composed the Master's Thesis independently, that no source materials or aids other than those mentioned have been used and that all citations have been declared appropriately.

Santiago, August 1st, 2018

Signature

Contents

1. Introduction 8
2. Theoretical frame 10
   2.1 Plasma focus devices 10
      2.1.1 Geometry types 11
      2.1.2 Plasma dynamics 12
   2.2 Radiation emitted by a PFD 14
      2.2.1 X-ray emission 15
      2.2.2 Neutron emission 18
      2.2.3 Applications of emissions from PFDs 20
   2.3 Strategies to characterize PF device emissions. 21
      2.3.1 Photomultiplier tubes (PMTs) 21
      2.3.2 Thermoluminiscent dosimeters 22
      2.3.3 Gas-filled detectors 28
         2.3.3.1 Ionization chamber 28
         2.3.3.2 Proportional counters (^{3}He proportional detector) 30
      2.3.4 Radiochromic films (EBT2) 31
   2.4 X-ray emission 32
      2.4.1 X-ray attenuation 33
      2.4.2 Effective energy 34
      2.4.3 Homogeneity coefficient 35
      2.4.4 Square inverse law 35
      2.4.5 Radiation protection 36
3. Materials and methods 38
   3.1 PF2kJ device 38
   3.2 X-ray emission 40
      3.2.1 Detectors 40
         3.2.1.1 PMT+ scintillator (PMTS) 40
         3.2.1.2 TLD 100 42
         3.2.1.3 Radiochromic films 44
         3.2.1.4 Ionization chamber (IC) 45
      3.2.2 Measurements 45
         3.2.2.1 Pressure efficiency for X-ray emission 45
         3.2.2.2 Device warming 47
         3.2.2.3 Output linearity study 47
         3.2.2.4 Spatial distribution study 48

3.2.2.5 Virtual source study 49
3.2.2.6 HVL and effective energy study 51
3.2.2.7 Radiation protection 52
3.3 Neutron emission characterization 53
3.3.1 Neutron detectors 54
3.3.1.1 ^{3}He proportional counter 54
3.3.1.2 TLD600-700 dosimeters 55
3.3.2 Neutron measurements 56
3.3.2.1 Pressure efficiency for neutron emission 56
3.3.2.2 Output linearity 56
3.3.2.2.1 TLD response varying the number of discharges 57
3.3.2.2.2 TLD response varying the moderator thickness 58
4. Results and Discussion 58
4.1 Dosimeters 58
4.1.1 Intrinsic sensitivity factor (ISF) 58
4.1.1.1 TLD 100 59
4.1.1.2 TLD 600 and TLD 700 59
4.1.2 Calibration factor (CF) 60
4.1.2.1 TLD 100 60
4.1.2.2 TLD 600 and TLD 700 61
4.2 X-ray emission 62
4.2.1 X-ray emission efficiency as a function of pressure variations 62
4.2.2 Device warming 64
4.2.3 Output linearity 65
4.2.4 Spatial distribution 68
4.2.5 Virtual source study 71
4.2.6 Effective energy 73
4.2.7 Radiation Protection 77
4.3 Neutron emission 79
4.3.1 Pressure efficiency for neutron emission 79
4.3.2 Neutron emission measurements 80
4.3.2.1 TLD600-700 response varying the number of discharges 80
4.3.2.2 TLD600 and TLD700 responses varying the moderator thickness 82
5. Conclusion and outlook 87
Bibliography 90

1. Introduction

Plasma focus (PF) devices started to be studied around 1960 by Filippov et al. in the USSR [1] and by Mather in the USA [2]. At the beginning these devices were famous since they were the most intense neutron emitting device in the field of controlled thermonuclear research.

A PF is a device in which a highly pulsed voltage is applied to a low pressure gas contained between coaxial cylindrical electrodes producing a dense plasma column that generates beams of ions and electrons, and x-ray pulses. If the discharges are perfomed using Deuterium gas, PF devices produce fast neutron pulses (~2.5 MeV) via fusion D-D reactions. Thus, the PF becomes a device well suited for applications since it reduces the danger of contamination compared with conventional radioactive sources of fast neutrons that emit continuously causing handling and storing problems.

PF devices became over time a essential tool for basic science research as astrophysical plasma research [3] as well as a device used in various applications in other areas such as neutron radiography [4], neutron activation analysis [5], X-ray radiography [6], hard X-Rays for brachytherapy [7] and hard x-ray radiation for flash radiography of metallic pieces [8]. A particular interest has also arisen in biological research of cancer cell response since PF devices are a source of pulsed x-ray emission [9].

Due to the several applications of these devices, the characterization of the pulsed x-ray and neutron emissions generated in dense plasma conditions has gained importance. Thermoluminescent dosimeters (TLDs), radiographic films, scintillator-photomultiplier systems and proportional detectors are some of the radiation detectors that have been used for this aim. Dose per pulse and spatial distribution of the x-ray emission have been measured by using TLDs [7], [10]-[11]. The effective energy of soft and hard x-rays has also been estimated in PF devices by means of x-ray transsmission measurements through different thicknesses by using usually radiographic films [8] [12] [13], as well as the energy

of neutron emission by means of the time-of-flight technique using photomultiplier detectors [14].

The dose level at which a operator and research staff may be exposed by these PF devices has arise as a concerning issue, being important to include it as part of the characterization of the PF devices [15], [16].

Due to the interest in these devices regarding the study of basic sciences and their potential applications, as it has already been mentioned, the emission generated by the plasma focus device (PFD) PF2kJ, from the Department of Thermonuclear Plasma from the Chilean Comission of Nuclear Energy (CCHEN), is studied in this thesis. The characterization of the emission from PF2kJ is defined as main objective in this work, which consist in the determination of the spatial distribution, the study of the reproducibility of the emission, the determination of the effective energy and the study of the variation of emission intensity as a function of distance for the x-ray emission. In addition, the x-ray exposure levels regarding radiation protection of the device operators are determined in order to be compared with the dose constraints required by national regulations and suggested by organizations concerned with radiation protection such as ICRP (International Commission on Radiological Protection).

With regard to neutron emission characterization, it is intended to determine the filling pressure that maximize the neutron emission and to perform preliminar measurements of output for being the base for future characterizations.

In the first part of this thesis work an introduction to PF devices, characteristics of the emission, and working principles of the radiation detectors used for characterizing the emission are given. Then, the measurements carried out and the specific characteristics of the radiation detectors used are described below. After, the results of the characterization of the emission of the PF2kJ are presented and analyzed. At last, some conclusions and possible future research works are exposed.

2. Theoretical frame

2.1 Plasma focus devices

A plasma focus device (PFD) is fundamentally a pulsed electric discharge system. In a PFD, the plasma is confined by magnetic field produced by the current generated in the own capacitor bank. This is possible due to the fact that plasma has a high percentage of charged particles. It is composed of two coaxial electrodes separated by an insulator sleeve around the base of anode which reside inside a vacuum chamber. The electrodes are connected to a pulsed power generator composed of a capacitor bank and a high-voltage switch. The overall layout of PF device with its various subsystems is shown as a block diagram in Figure 1.

The whole PF system is operated at optimal pressure ranges which satisfy the focusing or pinching of the plasma sheath. The vacuum condition allows for reliable sheath formation in the initial stage as the minimum breakdown voltage depends on the pressure following Paschen's law [17]. The insulator sleeve placed around the base of the anode allows proper formation of the plasma sheath in the initial breakdown phase and leads to efficient pinching [18]. To operate the plasma focus, high-voltage (typically greater than ten kV) and high-current (>10 kA) electrical pulses of few hundred ns to few μs duration are required. These pulses are generated by charging a capacitor to a suitable voltage and discharging it through the plasma focus. The discharge generates high density plasma of a short duration and subsequently ions, electrons, x-rays pulses and also neutrons are produced. The typical working gases used in most PF devices are hydrogen, deuterium, inert gases, and reactive gases such as oxygen, nitrogen, methane, acetylene, etc. Most studies that require the production of radiation (X-rays or neutrons) sources utilize inert or deuterium gas.

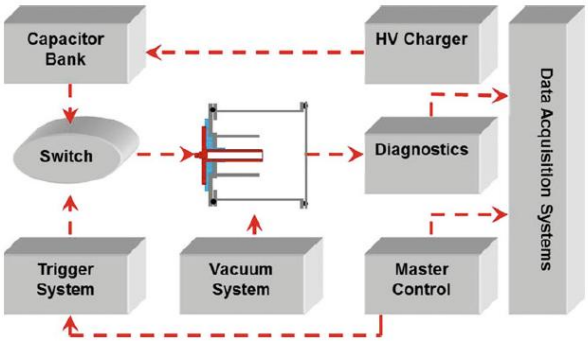

Figure 1: Block diagram representation of a PF device. Each block depicts: PF chamber at the center; High Voltage (HV) charger needed to charge the capacitor bank; triggerable high-current switch(es) (Switch+Trigger System) to transfer energy from the bank to the load (electrode assembly in PF chamber) at a preset voltage and time; devices (diagnostics) to measure the several radiation emissions and current/voltage signals from the device; and data acquisition system. Figure taken from [19].

2.1.1 Geometry types

There are two types of PF devices regarding the electrodes geometry: Filippov geometry [1]**,** which is characterized by a small aspect ratio of the anode (length/diameter< 1) and the Mather geometry [2], characterized by a big aspect ratio (length/diameter > 1) (see Figure 2). In this work, a Mather geometry device is studied. Nonetheless, both types of PFDs have similar working principles.

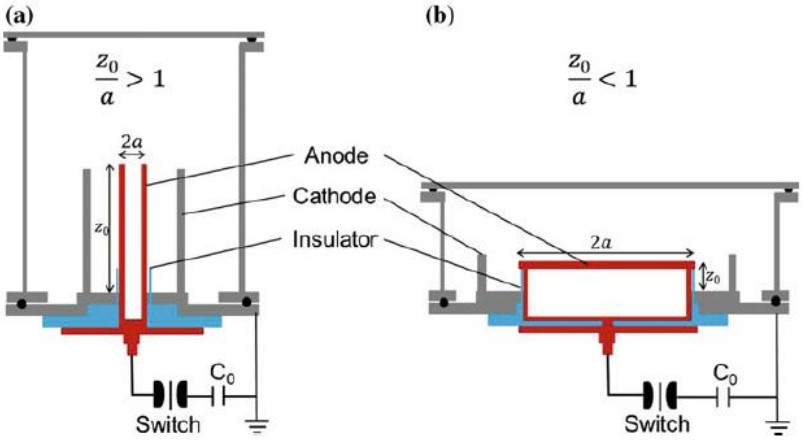

Figure 2: Schematic dense plasma focus device (a) Mather-type and (b) Filippov-type. Figure taken from [19].

2.1.2 Plasma dynamics

The PF chamber is first evacuated to a base pressure by using a pump. The working gas is then filled up to the right operating pressure range which is different for different gases (typically about few mbar). The capacitor bank is then charged to high voltages (typically in the 10–30 kV range) using a high-voltage power supply. The electrical energy stored in the capacitor bank is then transferred to the electrode assembly resulting in gas breakdown in the PF device chamber, which undergoes several phases. These are briefly explained below, for the Mather type-devices. The four distinct phases of the dynamics of the plasma focus discharge are depicted in Figure 3.

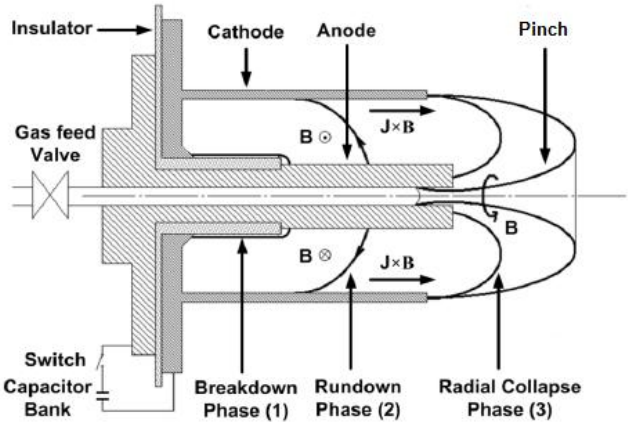

Figure 3: Different phases of plasma dynamics from (1) breakdown and current sheath formation, (2) axial acceleration, (3) radial compression and pinch phase. The post pinch phase is not shown here (disruption phase). Figure source [19].

2.1.2.1 Breakdown phase

First, a high pulsed voltage is applied between the electrodes of the PF device producing a dielectric breakdown of the filling gas over the insulator. This creates a strong electric field between the electrodes. The ionization of the gas grows exponentially due to free electrons under the influence of the electric field. These ionize the neutral particles and release bound electron which become free electron for subsequent ionization. Thus, the number of free electrons increases rapidly forming an avalanche that leads to the formation of the current sheath which connects the anode with the bottom of the cathode.

2.1.2.2 Axial rundown phase

Formation of the plasma current sheath in the breakdown phase provides a current density $\vec{J}$which, in turn, provides an azimuthal magnetic field $\vec{B}$. The z-component of Lorentz force ($\vec{J} \times \vec{B}$) pushes the sheath towards the open end of the anode and the radial component towards the outer cathode. The current sheath is accelerated in a canted profile by the Lorentz force since the magnetic field is more intense at the surface of the anode but weakest at the cathode (magnetic field has 1/r dependence). In this axial acceleration phase, the current sheath sweeps the neutral gas particles inside and heats them to form plasma which grows in density. After a short period, the current sheath tends to move with a roughly constant axial velocity. This velocity is in the range of 1.7 to 15 cm/μs [20].

2.1.2.3 The radial compression phase

When the current sheath reaches the end of the anode, it is now accelerated radially inward by the Lorentz force. This radial acceleration leads to a fast compression of neutral gas by the plasma current sheath generating radial shock waves, which ionize the gas and produce plasma at the top of the anode. This is how the plasma column is formed (pinch phase). The minimum radius and the lifetime of the pinch depends on the anode radius [21]. The gas trapped in the focused plasma is about 10% of the total volume swept by the current sheath [22] . In this phase, the current sheath velocity is higher than axial velocity. The radial velocity is around 25cm/μs [20]. At the end of this phase the magnetohydrodynamic (MHD) instability induces a gradual disruption of the plasma column due to increasing electron temperature.

2.1.2.4 The disruption phase

This phase starts when the plasma column is perturbed by instabilities which mechanisms are not clear yet. Hypotheses relate this phase with MHD [23] and Rayleigh-Taylor (RT) instabilities. RT is the instability of an interface between two fluids of different densities, which occurs when the lighter fluid is pushing the heavier fluid [24]. Due to these instabilities, charge particles are accelerated producing x-rays

via bremsstrahlung and also neutrons by beam-target fusion mechanism if filled gas is deuterium. How these emissions are produced is explained in the Section 2.2.

In order to ascertain electrical performance and discharge phenomena in the PF device, a current derivative probe (Rogowski coil) that measures the time derivative of the discharge current (dI/dt) and a calibrated fast resistive voltage divider that is used for measuring the voltage evolution between electrodes, are used. These electrical signals of the discharge are taken as references for the time scale and for describing the evolution of the current sheet bridging the electrodes. Hence, the different plasma phases can be distinguished. A dip in the current derivative signal indicates good formation of the plasma column and its minimum level defines the moment of pinch [25]. A spike observed at voltage signal is the evidence of pinching action in PF discharges [26] (see Figure 4).

In this work, it was considered that the device was ready to be used for an efficient radiation emission when the dip and the spike are identified during the device warming, indicating that a good pinch effect is reached.

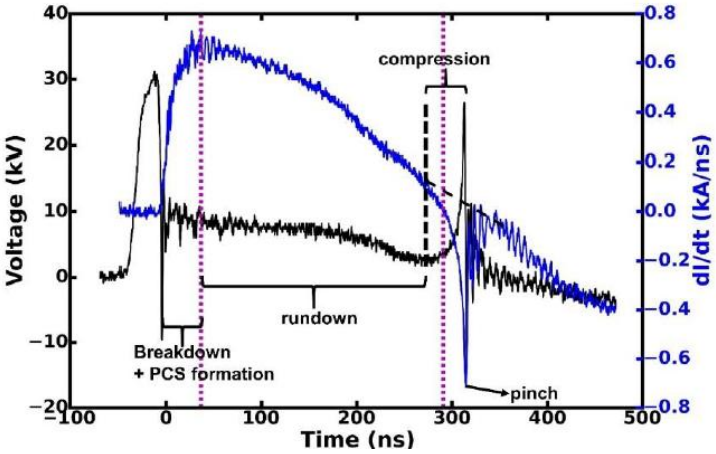

Figure 4: Current derivative and voltage diagnostic signals from Rogowski coil and voltage divider respectively. The different plasma phases are indicated. Figure source [27].

2.2 Radiation emitted by a PFD

The PFD is a source of energetic ions, relativistic electrons and electromagnetic radiation extending from infrared to hard x-rays, as well as neutrons, when it is

operated in deuterium medium [28]. The instability formation, which takes place during the end of radial plasma phase, causes a charge particle beam emission [29] (ions and electrons) where the particles are accelerated in the directions shown in Figure 5. The interaction of these particles with the plasma and electrodes generates neutron and x-ray emissions.

In the next sections the production of these two kinds of emission generated by a PF device will be described. The characterization and description of ion or electron beams are not described here, although research work related to this topic can be found in more detailed in several previous works as [29], [30] and [31].

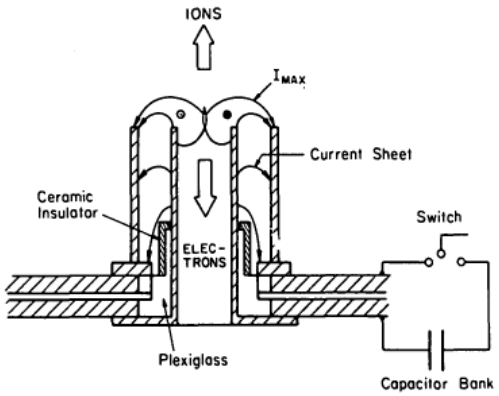

Figure 5: During pinch time the ions and electrons are accelerated in directions shown. Scheme taken from [32].

2.2.1 X-ray emission

The emission of X-rays in the PFDs was initially studied related to the emission of neutrons [33]. These devices produce hard x-rays (10-100 keV) and soft x-rays (1-10 keV) [12], and it has been stated that they are produced by the following processes in a PF device.

Two x-ray sources in the focus can be distinguished during plasma dynamics. The first is the result of thermal processes inside the plasma which leads to soft x-ray production via bremsstrahlung (free–free transition of electrons and ions interacting in the Coulomb field); recombination (free electron loses its energy on recombination with an ion) and line radiation (bound electron loses energy by falling into a lower energy state). The spectrum of this source varies with time of emission, the distance

along the focused column and with the amount of high-Z contamination in the gas [34].

The second is the result of non-thermal processes which leads to hard x-ray production. The production is attributed to electron bombardment of the centre positive electrode by the conduction electrons in the current sheath. Hence, the emission is related to bremsstrahlung and line emission processes. The characteristics of this source are similar to those of a high voltage X-ray tube thus the hard x-ray characteristics are determined by the parameters of the electron beam (the duration, current, and energy of accelerated electrons) and the properties of the characteristic x-ray emission of the anode material [35].

Some characteristics founded in PF devices are that the x-ray yield depends on the total voltage drop in the forming pinch but not on the anode length [36]. In order to achieve the best (x-ray/neutron) emission efficiency, the maximum pinch compression should be close to the peak current [13]. This can be achieved by modifying the filling gas pressure or the electrodes geometry. Regarding to shot-to-shot reproducibility of X-ray emission, generally it is poor because of the multiple parameters affecting the emission spectrum [34].

It is also mentioned in [34] that secondary X-ray pulses can be produced in one discharge and this phenomenon is common in plasma focus experiments. It is believed that they result from an adiabatic recompression of some part of the focused column, produced by the tube voltage fluctuations.

Knowledge of the hard x-ray effective energy of PF devices is important for the development of applications and also for cross-checking complex issues associated with physical processes occurring in the focus. For this reason, effective energy of X-ray emission has been measured in several PF devices. Some values are shown in Table 1. They have been generally obtained from determination of an effective mass attenuation coefficient. In order to determine it, measurements of the X-ray transmission through different thickness of materials are performed by using some radiation detector as thermoluminescent dosimeters or radiographic films. X-ray emission spectrum has been also determined by differential absorption-based

techniques, where the transmission values are used to infer an effective spectrum by the zeroth-order regularization method [37].

Table 1: Effective energy values of x-ray emission generated by several PF devices. The energy of the capacitor bank of the device, the filling gas and the method used for determining the effective energy or spectrum are specified.

Autor	Device energy & filling gas	X-rays energy	Method
C. Moreno *et. el.* [38]	4.7 kJ Gas: deuterium mixed with 2.5 % of argon.	Effective energy of 102±10 keV.	Transmission measurements by radiographic x-rays film with various thicknesses of metallic filters
Zambra *et. al.* [12]	400J Gas: Hydrogen	Effective energy ranging from 36 to 118 keV.	Transmission measurements by radiographic x-rays film with various thicknesses of metallic filters, when Ag and Pb target are placed in the anode to enhance the radiation.
Angeli *et. al.* [39]	7kJ Gas: Hydrogen	Peak of the x-ray spectrum at 10 keV	Calibrated LiF TLD dosimeters at 59.54 keV are used for transmission measurements and differential attenuation technique to determine spectrum
Knoblauch *et. al.* [40]	2.5 kJ Gas: Deuterium	Effective energy of 83±10 keV	Transmission measurements by radiographic x-rays film with various thicknesses of metallic filters
Raspa *et. al.* [8]	5.7kJ Gas: Deuterium	Spectral components in the 40-150 keV range, with a single maximum around 60-80 keV	Differential absorption method to determination of spectrum by performing attenuation measurements on metallic samples using commercial radiographic film.

2.2.2 Neutron emission

The PF, when discovered, was attractive for researchers due to the intense bursts of neutrons emitted from the $^{2}H(d,n)^{3}He$ fusion reaction, when the device is operated using deuterium gas**.** Several experimental investigations have been performed in order to understand the nature of fusion mechanism and to test the validity of the proposed models that may explain the neutron emission.

There are two main different mechanisms that explain neutron production in the PF device, when the filling gas is deuterium. The first is the thermonuclear mechanism. Here, the deuterium ions are approximately in thermal equilibrium with one another and collide inside the bulk of plasma column. The second process is the suprathermal mechanism, where beam-target [41] and gyrating particle [42] models are the two models considered although the most accepted is the first one. In beam-target model, accelerated deuterons strike ions at rest. In spite of thermal mechanism and beam-target mechanism are the two most accepted for explaining neutron production, the beam-target model has a more important role in PF devices since presence of the thermonuclear neutrons is supposedly restricted due to lower lifetime of plasma column. Moo et al [43] have shown that the neutron yield produced by beam-target mechanism is of the order of six times higher than the yield produced by thermal mechanisms in conventional plasma focus machines.

Time-of-flight (TOF) method has been used in order to estimate neutron emission energy from a PF device [14]. Detectors are placed in the same direction at different distances from the source, and the delay time of the signal taken from each one is used to estimate the neutron energy by its kinetic energy. The neutron spectrum was measured in a 490kJ PF device by using nuclear emulsion plates technique [44]. There, the peak energy was 2.85 MeV in the axial direction. Neutron energy values from other devices are shown in Table 2. Based on the values shown, it can be roughly estimated a neutron energy around 2 to 4 MeV for PF devices in axial direction.

Axial and radial neutron emission anisotropy is a general behaviour of PF device. Some anisotropy values are shown in Table 2. Anisotropy is also noticed in neutron energy.

Table 2: Values of neutron yield per shot in the axial direction, anisotropy and energy of neutron emission generated by some PF devices. The energy of the capacitor bank of the device is also indicated.

Device	**Device energy (kJ)**	**Neutron Yield**	**Anisotropy yield Y(0°)/Y(90°)**	**Energy (MeV)**
PF-2.2kJ; Talukdar et al [45]	2.2	8.27×10^{6}	1.25	R: 1.77-2.75 A : 1.89-3.93
PF-400J; J. Moreno et al [14]	0.32	$(1.06 \pm 0.13) 10^{6}$	1.5±0.3	R: 2.40 ± 0.03 A: 2.84 ± 0.11
PF-50J; Soto et al [46]	0.05	$(1.2 \pm 0.5) 10^{4}$	--------	A: 2.7±1.8
SPEED 2; Soto et al [13]	67	10^{10}-10^{11}	--------	---------
PF-1MJ ; Milanese & Pouzo [47]	1000	10^{11}	----------	R: Peak of spectrum 2.45 MeV

R: radial direction
A: axial direction

On the subject of shot-to-shot reproducibility of neutron emission, in all the devices, neutron yield values fluctuate on a shot to shot basis under apparently identical operating conditions (electrodes geometry, voltage, pressure); but it is not clear why this occurs [26].

2.2.3 Applications of emissions from PFDs

The pulsed neutrons and X-rays of PFDs have found applications in various fields such as neutron radiography [4]**,** neutron activation analysis [5], research of potential PF use in medical applications [48], X-ray radiography [6], hard X-Rays suitable for interstitial radiosurgery [7], hard x-ray radiation for flash radiography of metallic pieces [40], biological research as cancer cell response in a pulsed source [9], among others uses. Due to these several applications, a dosimetric characterization of PF sources becomes important, in order to assess a dose output as well as to ensure a safe environment for device operators and research staff.

Some dosimetric measurements have been performed in several works as Knoblauch et al [10], where a PF of 4.7kJ of stored energy delivers an average dose of 53 ± 3 μGy/shot on axis at 53 cm from the hard x-ray source. The emission is assessed by TLD700 and x-ray dose angular dependence is also characterized.

The output of a 2kJ PF device has been determined by TLD200 where the hard x-ray emission is 0.1 mrad/shot at 1m from the focus [49].

The x-ray dose measurements were carried out in presence of neutrons in all the works mentioned above.

X-ray dose values have also been reported when x-rays are emitted only. Tartari et al. [7] measured the dose of a PF device intended to assess its feasibility to act as an interstitial radiosurgery probe, where 4.5Gy/shot at 10 mm from the x-ray source was obtained. Here, the x-ray source comes from the relativistic electron beams exiting the PF chamber that impinging a tungsten target at 10 cm far from the rear of the PF head.

An average equivalent dose of few tenths of Sievert per shot was measured by Zarpyanov et al. [50] inside the chamber of a 3kJ PF device. Dubrovsky et al. [11] obtained dose values per shot of 10^{-5}-10^{-2}Gy in a PF 2kJ device and around of 10^{-6}-10^{-3} Gy in a PF of stored energy of 100J. TL dosimeters (LiF:MgCuP) were placed at

20 cm from PF chamber in both devices. In addition, equivalent dose of 17μSv per shot was estimated in a PF 400J device at the axial direction by using TLD100 [25].

In addition to dosimetric characterization measurements**,** X-rays pulsed emissions of PF may be promising candidates for reference studies in regard to standards for calibration and use of dosimeters in pulsed radiation fields [51]**,** [52].

2.3 Strategies to characterize PF device emissions.

PFDs as well as other similar pulsed discharge devices require a variety of diagnostics for their proper control and optimization, including the detection of X-rays and neutron emissions.
Radiation detectors that were used to characterize the x-ray and neutron emissions produced by the PF device PF2kJ are described in this section.

2.3.1 Photomultiplier tubes (PMTs)

A photomultiplier tube is a vacuum tube device that converts light into a measurable electric current. It consists of an input window, a photocathode, focusing electrodes, an electron multiplier and an anode. Figure 6 shows a schematic diagram of typical photomultiplier. The conversion starts when light passes through the input window and reaches the photocathode where it excites the electrons there. Then, incident light is converted into a current of electrons by the photoelectric effect. These photoelectrons are emitted into the vacuum and then they are accelerated and focused by the focusing electrode onto the first dynode, where they are multiplied by means of secondary electron emission. This secondary emission is repeated at each of the successive dynodes. The multiplied secondary electrons emitted from the last dynode are finally collected by the anode producing an electrical signal which can be recorded by an oscilloscope system.

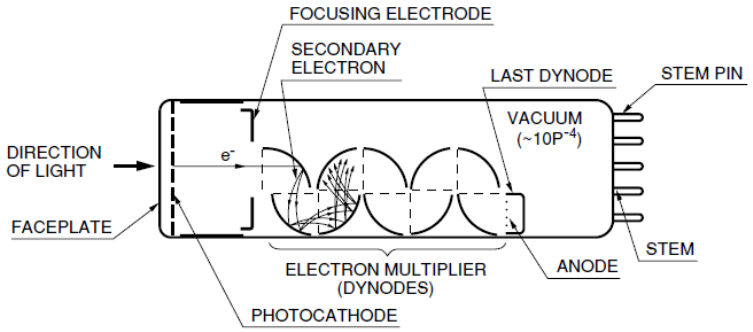

Figure 6: Schematic diagram of a photomultiplier. Image taken from [53].

In order to detect radiation emission (hard x-rays and neutrons) a scintillation detector is usually optically coupled to a PMT. As radiation passes through the scintillator, it excites the atoms and molecules making the scintillator to emit visible light. This light is transmitted to the PMT where is finally converted into an amplified electric signal as it was explained before. There are organic and inorganic scintillators. Organic crystals, organic liquids and plastics belong to the first category. A more detailed explanation about these detectors can be found in [54].

2.3.2 Thermoluminiscent dosimeters

Thermoluminescence is the thermally stimulated emission of light following the previous absorption of energy from radiation [55]. This phenomenon can be observed in thermoluminescent materials as insulators or semiconductors, where the wavelength of the emitted light is characteristic of the substance and not of the incident radiation.

The luminescence emission can be explained by the transfer of energy from radiation to the electrons of the solid, thus exciting the electrons from a ground state to an excited state. The emission of luminescence photon takes place when an excited electron returns to its ground state. However, whenever there are structural defects in a solid crystal, or if there are impurities within the lattice, there is a possibility for the electrons to possess energies which are forbidden in the perfect crystal where they remain in a metastable state until they are given them enough thermal energy to return to the conduction band from where it can undergo a normal transition back to the valence band (ground state). These energy traps are created in TL crystal

dosimeters by adding artificially impurities (doping) and which depending on the atomic species.

The energy band model as a means of interpreting luminescence phenomena in many phosphors has been especially useful in providing an understanding of processes which involve transport of an electronic charge through the lattice. The simplest model of energy band model is depicted in the Figure 7. It consists of two delocalized bands: conduction band (CB) with energy E_c, and valence band with energy E_v, and two localized levels (metastable states), one acting as a trap, T, and the other acting as a recombination center (R). The distance between the trap T and the bottom of the CB is called activation energy or trap depth E. This energy will be the energy required to liberate an electron, which is trapped in T.

It is convenient to separate the thermoluminescence phenomenon into two parts: one describing the trap filling during irradiation and one describing the trap emptying during thermal excitation.

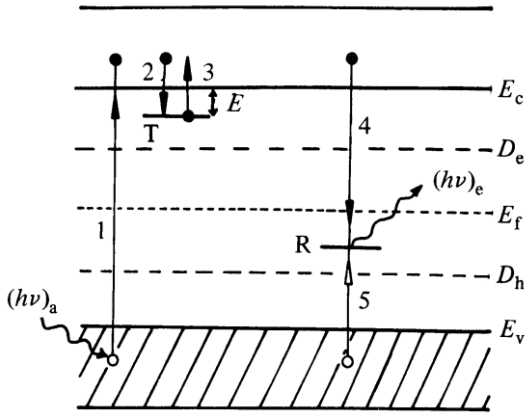

Figure 7: Two-level model for thermoluminescence. Allowed transitions: (1) ionization; (2) and (5) trapping; (3) thermal release; (4) radiative recombination and the emission of light. Electrons are the active carriers, but an exactly analogous situation arises for holes. Electrons, solid circles; electron transitions, solid arrows; holes, open circles; hole transitions, open arrows. Figure taken from [55].

During irradiation, absorption of radiation of energy (hv) > E_c - E_v produces free electrons in the conduction band and free holes in the valence band (transition 1). The free carriers may either recombine with each other or become trapped. The recombination occurs in an indirect way (it is a more likely process than direct). First, holes become trapped at centres (R) (transition 5) in order for the recombination to

occur. Then, recombination takes place via the annihilation of the trapped holes by free electrons (transition 4) and then luminescence results.

The free electrons may also become trapped at level T (transition 2) as was mentioned before. Here, recombination can only take place if the trapped electrons absorb enough energy E to be released back into the conduction band, from where recombination is possible. Thus, the luminescence emission is delayed by an amount governed by the mean time τ spent by the electrons in the trap, and it is based in the assumption that electrons follow a Maxwellian distribution:

$$\boldsymbol{p = \tau^{-1} = s \exp\left(-\frac{E}{kT}\right)} \quad (1)$$

Here, p is the probability of an electron escaping from a trap of depth E at temperature T. k is the Boltzmann's constant and the term s is called the frequency factor or attempt-to-escape factor that depends on the frequency of hits in the trap which can be considered as a potential well. s is considered as a constant (not temperature dependent considering the simple model).

The return to equilibrium can be speeded up by raising the temperature above irradiation temperature (T_o) such that E < kT. This in turn will increase the probability of detrapping and the electrons will now be released from the trap into the conduction band (transition 3). Thermoluminescence now results when the free electrons recombine with the trapped holes.

The emitted light due to a previously irradiated TL crystal that is heated can be detected by a photodiode and then converted into electric current to be quantified. The intensity of the emitted light is illustrated in so-called glow curves. The shape of the glow curves is given by the overlay of several glow peaks (see Figure 8) where the area under each glow peak curve is proportional to the number of electrons initially trapped and hence is proportional to the absorbed dose [56]**.**

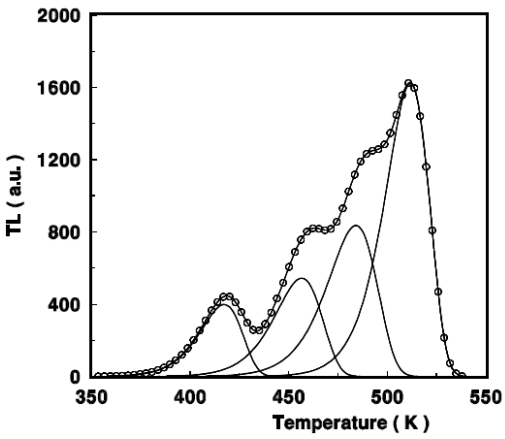

Figure 8: Glow curve (line with circles) given by overlay of glow peaks (lines). Taken from [57].

In regard to TL materials for dosimetry, Lithium fluoride (LiF) material is the 'standard' thermoluminiscence phosphor and it has been considered a useful material in dose measurement for several reasons, including its tissue equivalence and general resistance to corrosion and wears [58]. There are also other materials suited to quantify the dose. Some of them are Lithium borate, $Li_2B_40_7$, with and effective atomic number of this material of 7.4 gives an energy response very similar to water (the reference material in dosimetry), but a large increase in its thermal fading rate (and a decrease in sensitivity); or calcium fluoride CaF_2, naturally occurring as mineral fluorite that can thus be cheaply obtained but a problem of using is the complexity of its glow-curve (Schayes et al., 1967) and it is not water equivalent. If the requirements of low thermal fading and tissue equivalent are considered, the most appropriate TLDs are the crystals of LiF:Mg,Ti (Lithium fluoride doped with magnesium and titanium). They have an effective atomic number of 8.14, a linear response in a range of $5x10^{-3}$ to 10^2, a saturation level of 10^5 at which all traps are full or radiation damage occurs and a low thermal fading (5-10% per year) [59].

LiF:Mg:Ti solids have been used to measure different type of radiation depending on the lithium isotopes. Because of TLD100 crystals are usually suitable to measure x-ray radiation; they were used for studying x-ray emission from the PF device PF2kJ in this work. They are composed by natural LiF and corrections are needed to apply when they are calibrated in a source of different energy from the study source, due to they have different energy photon response [60] (see Figure 9).

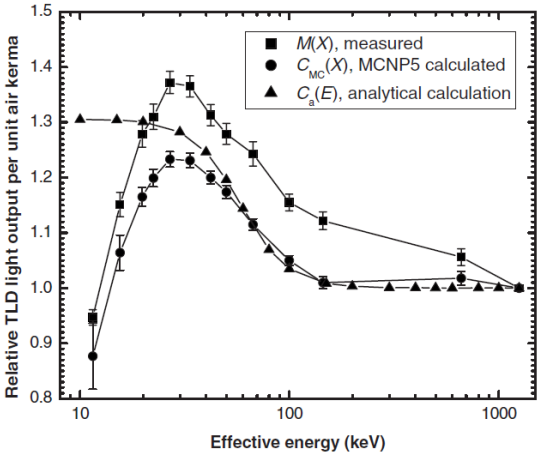

Figure 9: Measured TLD100 light output per unit air kerma as a function of photon energy M(X) as well as calculated dose to TLD100 per unit air kerma as a function of photon energy for the Monte Carlo $C_{MC}(X)$ and analytical $C_a(E)$ methods. All results are normalized to the response to ^{60}Co photons. Taken from [60].

Relative to dosimetry of mixed neutron-gamma radiation, it is usually performed with a pair of ^{6}Li and ^{7}Li dosimeters by these lithium isotopes. They are named TLD600 and TLD700 respectively. The first is sensitive to gamma and neutron radiation, and the second to gamma radiation only. ^{6}Li as a neutron dosimeter is based on the $^{6}Li(n,\alpha)^{3}He$ reaction, since neutrons have no charge, their detection relies upon the effects of the secondary particles. It has a higher cross section for thermal neutrons than fast neutrons (945 barns for thermal neutrons vs 0.3 barns for 1MeV neutrons) [61]. The TLD700 cross section for thermal neutrons can be neglected when it is compared with TLD600 (low cross section (0.033 b) of the reaction $^{7}Li(n, \gamma)^{8}Li$). Both dosimeters have the same sensitivity to gamma radiation. The composition and sensitivity to thermal neutrons are shown in Table 3. The sensitivity is determined as the response to a fluence of 10^{10} thermal neutrons per cm^2 in terms of an equivalent exposure to ^{60}Co gamma rays.

Table 3: Percentage of the Li isotopes ^{6}Li and ^{7}Li and sensitivity to thermal neutrons for TLD100, TLD600 and TLD700.

Phosphor	^{7}Li percentage	^{6}Li percentage	Sensitivity to thermal neutrons [62]
TLD 100	92.50	7.50	328
TLD 600	4.40	95.60	1360
TLD 700	99.993	0.007	1.1

In the present work, TLD100 dosimeters were used to monitor personal equivalent dose near the device for radiation protection purposes and for the characterization of the PF2kJ x-ray emission when filling gas was Hydrogen, while pairs of TLD600 and TLD700 were used as a first attempt to perform relative measurements in a mixed gamma-neutron emission when filling gas was Deuterium.

In order to use the TLDs as a dosimeter, a calibration is performed, which is the procedure to translate the crystal signal to dose values. The specifications of the calibration used for radiation protection can be found in the Radiation Protection section of Materials and Methods section 4.2.7. The net TL signal from each crystal (integral of the glow curve) after subtraction of intrinsic background (signal obtained from non-irradiated crystals), needs to be corrected by a relative intrinsic sensitivity factor that considers the response variation to the same irradiation within individual detectors. This factor also is used to select the dosimeters that respond within some established tolerance from the average, prior to their dosimetric use. It is calculated as:

$$S_i = \frac{\bar{M}}{M_i} \qquad (2),$$

where M_i is the net reading of the dosimeter I and M the average of the readings of all the dosimeters irradiated.

Also a proper correction in regard to energy response needs to be applied in the case of calibrating in a different energy spectrum as mentioned before.

For each TL material it is extremely important to know the procedure for restoring its basal conditions before a new irradiation. This procedure is called annealing and has two aims: the first is to empty the traps of the phosphor completely after the irradiation and readout cycle and therefore, annealing is performed before irradiation or after readout; the second is to stabilize the electron traps in order to obtain, within narrow limits, the same glow curves for the same dose even after repeated irradiations and thermal treatments. Additional annealing procedure can be carried out, in which the low-temperature peaks are erased because they are normally

subjected to a quick thermal decay and therefore they should not be included in the TL signal to avoid higher uncertainty in the dose determination. This annealing is performed before readout.

2.3.3 Gas-filled detectors

These detectors respond to radiation by means of ionization-induced electrical currents. They consist in a volume of gas contained between two electrodes having a voltage difference between them. When radiation passes through the gas causes ionization. The freed electrons are attracted to the positive electrode and the ionized atoms to the negative electrode, causing a momentary flow of a small amount of electrical current. Two gas-filled detectors are used in this work: an ionization chamber and a proportional counter.

2.3.3.1 Ionization chamber

The ionization chamber (IC) consists of an outer cylindrical electrode (metal or graphite coated in plastic) with a wire electrode running down its center. If little or no voltage is applied to the gas-filled detectors, most of the electrons will recombine and no electrical output signal is produced. If a positive voltage is applied to the anode, the electrons will move toward it and the positively charged ions will move toward the cathode. An electrical output signal will be produced whose magnitude depends on the applied voltage, the geometry of the counter, and the filling gas. These parameters determine whether the detector operates in the ionization chamber region, the proportional region, or the Geiger-Mueller region. These different operating regions are shown in the Figure 10.

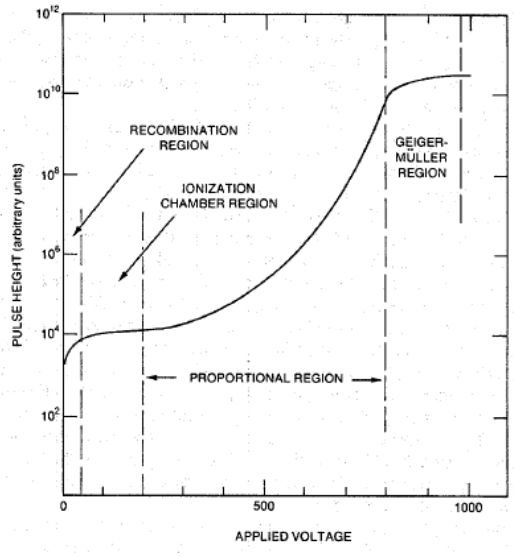

Figure 10: Pulsed-height against applied-voltage curves to illustrate ionization, proportional, and Geiger-Mueller regions of operation. Image taken from [63].

ICs work in the ionization chamber or saturation current region where the voltage required is enough to collect nearly all the electrons before they can recombine. At this point a plateau is reached and further small increases in voltage yield no more electrons. The charge collected is proportional to the energy deposited in the gas and independent of the applied voltage.

If the chamber used is open to the ambient air, the mass of air in the cavity volume is subject to atmospheric variations. Therefore, air temperature and pressure correction (k_{TP} factor) is needed to correct the IC signal. If T_0 = 20°C (or 293.2° K) and P_0 = 101.3 kPa are the reference conditions for chamber air temperature and pressure, T and P are the actual air temperature (in °C) and pressure (in kPa), then, due to the ideal gas physical law, the correction factor for air temperature and pressure k_{TP} in the user's beam, is [64]:

$$\boldsymbol{k_{TP} = \frac{(273.2+T)\,P_0}{(273.2+T_0)\,P}} \tag{3}$$

For x-rays and gamma rays, the ionization chamber response changes with photon energy because photon absorption in the gas volume and in the chamber walls and relative penetration of photons through the chamber walls are both energy-dependent processes. Figure 11 shows a typical energy-response curve.

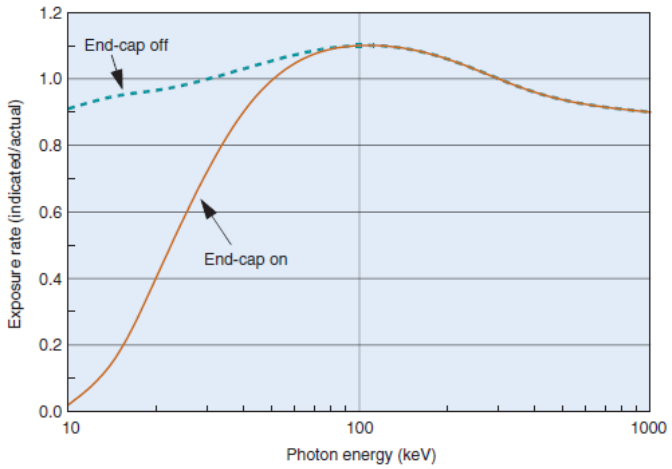

Figure 11: Energy response curve for a typical ionization chamber survey meter with and without a removable protective end cap. Image taken from [65].

2.3.3.2 Proportional counters (^{3}He proportional detector)

The proportional counters works in the region beyond the ionization chamber or saturation current (see Figure 10). Here, the electric field strength is large enough so that the primary electrons can gain sufficient energy to ionize the gas molecules and create secondary ionizations. If the field strength is increased further, the secondary electrons can also ionize gas molecules. This process continues rapidly as the field strength increases, thus producing a large multiplication of the number of ions formed after the primary event. This cumulative amplification process is known as avalanche ionization. In the proportional region the charge collected is also linearly proportional to the energy deposited in the gas [65] .

Mechanisms for detecting neutrons in matter are based on indirect methods since they are neutral and they do not interact directly with the electrons in matter. The process of neutron detection begins when neutrons, interacting with various nuclei, initiate the release of one or more charged particles. The electrical signals produced by the charged particles can then be processed by the detection system and in this way the presence of neutrons can be deduced. For this purpose, two basic types of neutron interactions with matter are available. First, the neutron can be scattered by a nucleus, transferring some of its kinetic energy to the nucleus. If enough energy is transferred the recoiling nucleus ionizes the material surrounding the point of interaction. Second, the neutron can cause a nuclear reaction. The products from

these reactions, such as protons, alpha particles, gamma rays, and fission fragments, can initiate the detection process. Then, it is possible to detect either thermal neutrons via nuclear reactions or fast neutrons via recoil interactions.

Gas-filled proportional detectors usually use ^{3}He gas for detecting thermal neutrons. The nuclear reaction that takes place here is:

$$^{3}_{2}He + n \rightarrow ^{3}_{1}He + p \qquad Q = 0.764\ \text{MeV}$$

This reaction is exothermic and release energetic charged particles into the gas. The cross section for this reaction is 5330 barn for thermal neutrons (~0.02 eV). Then, it is customary to embed the ^{3}He detector in polyethylene material or other moderating materials to maximize their counting efficiency [66].

2.3.4 Radiochromic films (EBT2)

In general, film dosimetry is a 2-dimensional dosimetry method with a high spatial resolution where the principle is the change of optical absorbance (optical density) when irradiated with ionizing radiation. Optical density can be measured with transmission film scanners. The intensity of the film scanner light is attenuated exponentially when transmitting through the film.

The change of optical absorbance of the film in response to radiation exposure is characterized by the net optical density that is given by:

$$netOD = -log_{10}\left(\frac{I}{I_0}\right) \tag{4}$$

where I_0 and I are the reading for the unexposed and exposed film piece, respectively.

Radiographic and radiochromic films are two film types to perform film dosimetry which operates with different principles. Since radiochromic films are used in this work, radiochromic dosimetric principle is explained only. It is a radiation induced polymerization process in the active component of the film that changes the optical absorbance. The active layer of the film is composed by monomers called

diacetylene with attached radicals. When the films are irradiated, they attach by linking up resulting the polymer polydiacetylene [67].

Radiochromic films are available with different structure, although all of them have the same radiation sensitive component [68] therefore; the radiochromic dosimetric principle is the same in all of them. They are EBT, EBT2 and EBT3. EBT has a double active layer structure. Then EBT was discontinued and replaced by EBT2 film that has a single active layer instead of double and yellow marker dye is added in this layer for uniformity corrections. The last version of these radiochromic films is EBT3 that has symmetrical layer configuration with a special surface treatment to prevent the formation of Newton rings during film scanning [67].

In general, EBT's exhibits highest sensitivity (higher absorbance) at 636 nm; therefore, if the film is scanned, the maximum sensitivity is obtained by using the red channel [69]. Film scanner response is affected by the scan orientation (portrait/landscape orientation) of the EBT and EBT2 films. For this reason it is critical to always scan EBT2 films in the same orientation. The reason is the anisotropic light scattering of the needle like structure of the active component (monomers), then more light is scattered perpendicular to the coating direction than parallel to the coating direction. Small energy dependence has been observed when the EBT2 film is scanned in the red component of a desktop scanner light source, in an energy range from 50 kVp to 10 MV [70]. Since EBT2 film is going to be used to measure spatial distribution of the x-ray emission generated by a PF device, a dose calibration is not required.

2.4 X-ray emission

In order to characterize the x-ray emission generated by PF2kJ device, HVL, effective energy and virtual source position were intended to be determined. In the next sections, theory behind these concepts is described.

2.4.1 X-ray attenuation

The x-ray attenuation is the reduction of the intensity of an x-ray beam while it traverses matter. This reduction can be due to absorption process, where the energy is transferred from photons to atoms of the target, or it can be due to photon scatter.

For a monochromatic beam, the logarithm of the number of photons transmitted varies linearly with the thickness of the attenuating material while for a polychromatic beam that contain a spectrum of photon energies, the transmission through an absorber does not strictly following a linear variation due to photons of low energy are attenuated more rapidly than the higher energy photons when the polychromatic beam passes through an absorber. Therefore, both the number of transmitted photons and the quality of the beam change with increasing thickness of the absorber. From the comparison of the curves for mono energetic and polyenergetic beam show in the Figure 12, it can be noticed that for polyenergetic beam, the initial slope of the curve will be steep because the low-energy photons are attenuated, but, as the beam becomes more monochromatic, the slope will decrease.

The penetrating ability or quality of an x-ray beam is determined explicitly by its spectral distribution, which indicates the energy present in each energy interval. However, the HVL or half-value layer is the concept used most often to describe the penetrating ability of x-ray beams below 300 keV and the penetration through specific materials. The HVL is defined as the thickness of a standard material that reduces the exposure to one-half.

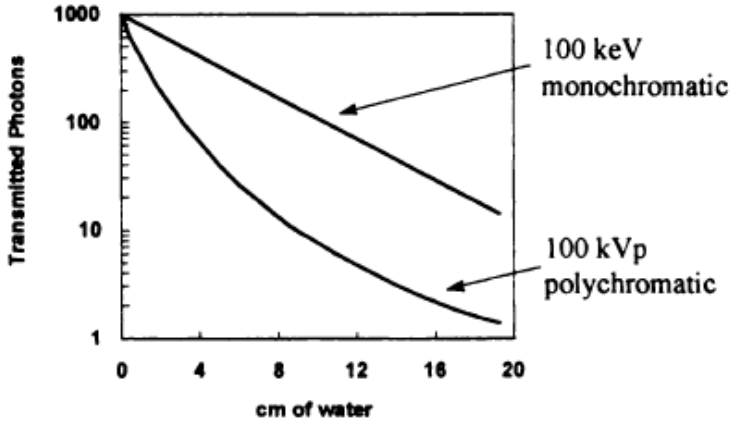

Figure 12: Comparison of the attenuation curves in water for polychromatic and monochromatic radiation. Taken from [71].

The HVL of an x-ray beam is obtained by measuring the exposure rate from the x-ray generator for a series of attenuating materials placed. These HVL measurements should be made under narrow-beam conditions or conditions of good geometry. When a broad-beam condition is present, a large number of photons from the absorber are scattered into the detector due to large x-ray beam is used and a small distance exists between the absorber and detector. Then, it will be indicated a greater penetrating power of the beam, which is not truly representative.

2.4.2 Effective energy

If the mass attenuation coefficients or linear attenuation coefficients for a given material are known, the effective energy of a polychromatic beam can be calculated. First, the “effective” linear attenuation coefficient is determined from the slope of the logarithm of the transmission (ln(I(x)/I(x=0)) against filter thicknesses x of attenuating material. Then, an interpolation of the values of energy and linear attenuation coefficients given in a tabulated data as [72] or of the mass attenuation curve for a given material as a function of energy, is performed.

The effective energy has been determined for X-ray emission of several PF devices. Some values and the method employed to energy determination can be founded in Table 1.

2.4.3 Homogeneity coefficient

The homogeneity coefficient is sometimes used in addition to the HVL as a descriptor of beam quality for polychromatic spectra. With a polychromatic beam, photons of low energy are attenuated more rapidly than photons of higher energy. The second HVL (i.e., the thickness required to reduce the penetration to one-quarter) is larger than the first HVL. The ratio between first and second HVL is called the homogeneity coefficient, i.e., HC=1st HVL/2nd HVL. It follows that the homogeneity coefficient for a polychromatic beam is less than one.

2.4.4 Square inverse law

If radiation is emitted isotropically from a point source, the total number of particles crossing the surface of a sphere of radius r centred on the source is independent of r. Therefore the particle fluence at a distance r, obtained by dividing this number of particles by the area of the surface of the sphere, varies proportionally to r^{-2}.

If L_1 and L_2 are the distances measured from the point of source and considering that the mentioned law is met, then the intensities at each distance I_1 and I_2 will be related as

$$\frac{\boldsymbol{I_1}}{\boldsymbol{I_2}} = \left(\frac{\boldsymbol{L_2}}{\boldsymbol{L_1}}\right)^{\boldsymbol{2}} \quad (5).$$

By using the expression in (5), an effective source position can be determined by measuring the output in air at several distances. Calling L_0 a reference distant from the physical source and S_v the virtual source shift from the physical source, then the expression above is:

$$\frac{I(L_0)}{I(L)} = \left(\frac{L+S_v}{L_0+S_v}\right)^2 \quad (6)$$

and therefore, by rearranging to get a linear relationship (y=mx+n),

$$\sqrt{\frac{I(L_0)}{I(L)}} = \frac{1}{(L_0+S_V)}L + \frac{S_V}{(L_0+S_V)} \quad (7)$$

2.4.5 Radiation protection

The device studied emits radiation and it is operated by researchers who may be exposed to some level of radiation. Hence, it is important to measure this exposure level and assess if it is within the dose limits recommended by international organizations that deal with Radiological Protection (e.g. ICRP) in order to prevent and limit harmful effects of radiation and also if it complies with national regulations (Supreme Decree N°3, 1985) [73].

Due to the fact that several plasma focus research projects are aimed at future medical applications (see section 2.2.3), exposure received by device operators has already begun to be evaluated. Fabbri et al. [15] performed an analysis of radiation protection of a plasma focus used for medical applications (short-lived radio nuclides breeding), suggesting several safety operational criteria. Monte Carlo simulations have also been performed [16] for the attenuation of neutron radiation produced at PF devices through various shielding designs in order to find the design that guarantee a safe environment according to level exposures accepted. Thermoluminescent dosimeters have been used for assessing exposure levels in these devices. El-Aragi et al. [74] measured x-ray emission as function of the applied voltage and filling gas by using TLD-500. The dose measured assuming the worst scenario, was compared with the dose limits for the whole body exposure of a radiation worker provided by ICRP (1990). It was obtained 15 mSv/y being below the limit suggested.

There are two main biological effects of radiation to be considered: tissue reactions (deterministic effects), which happen when the radiation dose exceeds a specific threshold and become evident days to months after exposure as they cause a predictable change in tissue, and stochastic effects, which relate to the potential future harm to the tissues and the body [75]**.** The stochastic effect of most concern is the carcinogenic effect. At low doses, where stochastic effects take place, cellular repair mechanisms will usually take place and the organism suffers no damage. However, the cellular repair process may be occasionally imperfect, with the result that cells retain their ability to replicate, but with coding damage to the DNA that causes the propagation of errors in succeeding generations of cells. The

consequence of this might ultimately be cancer, or if the somatic cells of the gonads are involved, the production of genetic effects in successive generations. For this reason, it is important to prevent the possible harmful effects of exposure to low doses through a control and monitoring of exposure to the personnel.

One of the most important organization concerned with radiation protection is the ICRP (International Commission on Radiological Protection), that is an international body whose remit is to function as an advisory body providing recommendations and guidance on radiation protection; others are IAEA (International Atomic Energy Agency), that deals specifically with the safe generation of nuclear energy and defines many of the procedures and criteria required; and the NCRP (National Council in Radiation Protection and Measurements) in USA. In Chile the main institutions concerned are CCHEN (Chilean Nuclear Energy Commission), ISP (Instituto de Salud pública, Institute of Public Health) SEREMI de Salud, and SOCHIPRA (Sociedad Chilena de Protección Radiológica, Chilean Society of Radiological Protection)[1]

There are special dose quantities adopted by ICRP with respect to Radiological Protection, which are used to specify dose values for limiting the occurrence of stochastic health effects below acceptable levels and avoiding tissue reactions in workers who are occupationally exposed and members of the public. These fundamental quantities of protection are based on the measurement of the energy deposited in organs and tissues of the human body. To relate the radiation dose to its risk, the variations in the biological effectiveness of the radiations of different quality, as well as the difference in the sensitivity of organs and tissues to the ionizing radiation have been taken into account.

These dose quantities in Radiological Protection are: radiation-weighted dose (or equivalent dose) in an organ or tissue (H_T), defined as the total energy imparted to specified organs and tissues divided by its total mass which requires then to apply suitably chosen weighting factors to take account of differences in biological effectiveness of different radiations; and the effective dose (E), which considers additionally the differences in radiation sensitivities of organs and tissues to

[1] More information about Radiological Protection Organizations/Institutions mentioned, can be obtained in ICRP at http://www.icrp.org; IAEA at http://www.iaea.or.at; CCHEN at http://www.cchen.cl/

stochastic health effects by a weighting factor. It is calculated by performing the weighted sum of the tissue-equivalent doses (H_T) and its unit is sievert (Sv) that is equal to Jkg^{-1}. The unit is the same for the equivalent dose and the effective dose, as well as for some the magnitudes of operational doses which are described below.

Since the equivalent dose and the effective dose cannot be measured directly in the tissues of the body, operational quantities [76] were created from which the equivalent organ dose and the effective dose can be evaluated. Operational quantities are aimed at providing a conservative estimate or upper limit for the value of the protection quantities related to an exposure, or potential exposure of persons under most irradiation conditions. They are measurable, and the instruments used to radiological monitoring then should be calibrated in terms of such magnitudes.

The operational quantities for area monitoring are the environmental dose equivalent, H*(10) and the directional dose equivalent, H (0.07, Ω). The operational quantity for individual external exposure is the personal dose equivalent, H_p (d) which is the dose equivalent in the ICRU (soft) tissue at an appropriate depth, d, below a specified point in the human body. Usually the point specified is that where the individual dosimeter is used. For the evaluation of the effective dose, $H_p(10)$ is chosen at a depth d = 10 mm, considering that the monitor dosimeter is used at chest level.

Regarding occupational exposure in planned exposure situations, ICRP recommends in the publication 103 [76] a limit of an effective dose of 20 mSv per year, averaged over defined 5 year periods (100 mSv in 5 years), with the further provision that the effective dose should not exceed 50 mSv in any single year.

It is important to know these dose constraints because they will be compared with the operational quantities measured during the operation of the the PF device in order to determine if additional security radiation protocols for operating the PF device will be required.

3. Materials and methods

3.1 PF2kJ device

The emission characterization was carried out on a Mather type PF device of 2kJ of nominal energy. This device (PF2kJ) was designed and constructed at the Chilean Nuclear Energy Commission (CCHEN). The schematic representation of a PF device was depicted before in Figure 1 and PF2kJ can be as well represented by it. It consists in a vacuum chamber, the electrodes inside of the chamber, a voltage divider (VDR) and a Rogowski coil as electric diagnostics, a capacitor bank, a charging unit, and a trigger switch system made up of a trigger plate, a trigger unit and spark gap. A PF2kJ scheme and some dimension specifications are shown in Figure 13.

There is a circular polyethylene window of 0.8 mm thickness and diameter of 4.5 cm at the top of the chamber and it is at 15 cm from the top of the anode, where the radiation emission can be detected. For additional settings, a lateral window of the chamber is available to measure radiation output as well. The ^{3}He detector was usually placed in that position.

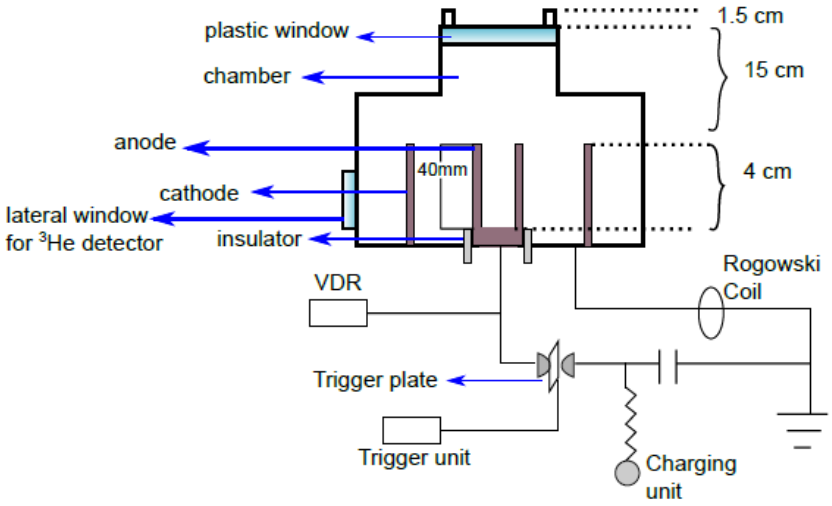

Figure 13: PF2kJ scheme and dimensions of the device.

Regarding electrodes, the central one is a hollow anode of radius and length of 12 mm and 50 mm respectively. An insulator of alumina partially covers it giving an effective anode length of 40mm. Twelve copper cathode bars of height 50 mm and radius of 30mm, symmetrically surround the central anode. Distance between this and cathode bars is 31 mm. Anode and cathodes are made of copper. The PF2kJ is powered by an 8μF capacitor bank operating up to 20 kV. A voltage divider (VDR) is connected to the central anode in order to trace typical PF discharge voltage signals.

A Rogowski coil, designed by winding two metallic wires loop connected electrically in the opposite directions, is mounted around the grounded cathode, outside PF-2kJ in order to measure the circuit current. A spark gap is connected to the central anode to create discharges inside the device. It consists of two semi spherical electrodes made of copper. The voltage in the capacitor bank ranges between 16 and 17 kV, with the spark gap operating in the self-breakdown regime. The spark gap is filled with Nitrogen gas and the pressure is set at 0.1 to 0.2 mbar in order to produce the discharges. They produce x-ray emission when the filling gas inside the device chamber is Hydrogen. On the other hand, a mixed emission of x-rays and neutron is produced if the filling gas is Deuterium.

It is important to mention that the device has a restriction in the number of consecutive discharges to avoid damage to the device, usually allowing consecutive shots of series of 20 to 30. In addition, since the device works at high currents that can induce overheating, it is necessary to restrict the number of discharges up 400 discharges on a day in order to prevent accidents regarding these issues.

3.2 X-ray emission

Different diagnostics are used in order to characterize the x-ray emission from the PF2kJ in this work. A scintillator-photomultiplier (PM) detector system, TLD100 dosimeters, EBT2 films and IC are used for this aim which will be specified in the first section. In the next section, the different studies performed regarding x-ray emission characterization are described.

3.2.1 Detectors

3.2.1.1 PMT+ scintillator (PMTS)

PMT and organic scintillators are used in order to characterize pulsed radiation emitted from the PF2kJ. The PMT used is R1828-08 (Hamamatsu) instrument coupled with bicorn BC-408 plastic scintillator with a diameter of 5 cm, thickness of 5 cm and with a optimized photon energy response range from 100 keV to 5 MeV. The PMT-scintillator (PMTS) detector system is placed at a distance of 140 cm from the

anode top. The setup is shown in Figure 14. The signal from the PMTS system is collected by a Tektronik TDS 684A oscilloscope. This oscilloscope also collects the signals from the VDR and the Rogowski coil. The software used to export the signals is WaveStar for oscilloscopes.

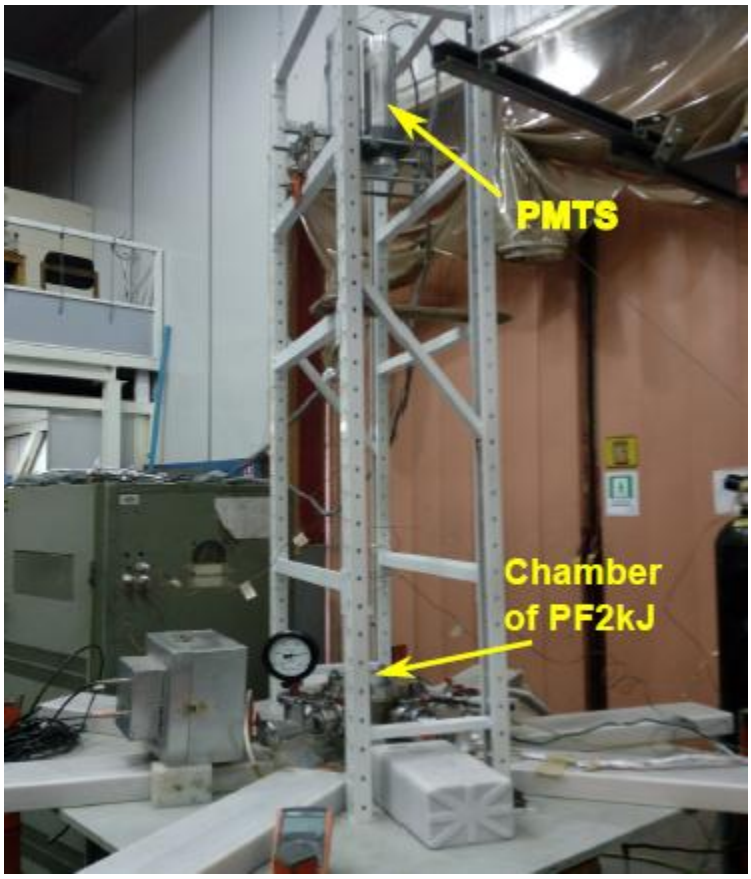

Figure 14: PMT-scintillator (PMTS) system setup. The distance from the base of the PMT to the top of the central anode is 140 cm.

The area under curve (a.u.c) of the signal due to x-ray emission detection by PMTS system is calculated by using a routine in Python provided by Jalaj Jain, who is a researcher at CCHEN. An integration example extracted from this program is shown in Figure 15. The red points are chosen to perform the integration and the result is given in V*s units. Sometimes a double signal is observed corresponding to two x-ray emissions (Figure 16). It has been previously reported [34] that this phenomenon can occur (see Section 2.2.1) and it must be considered in the PMT signal integration process.

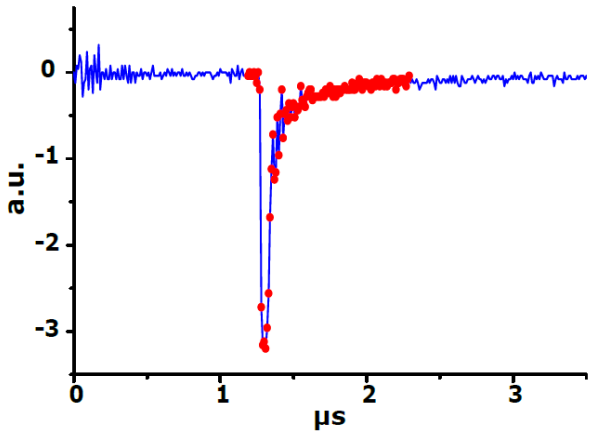

Figure 15: PMT signal integration example. The red points are considered to calculate the area of the signal.

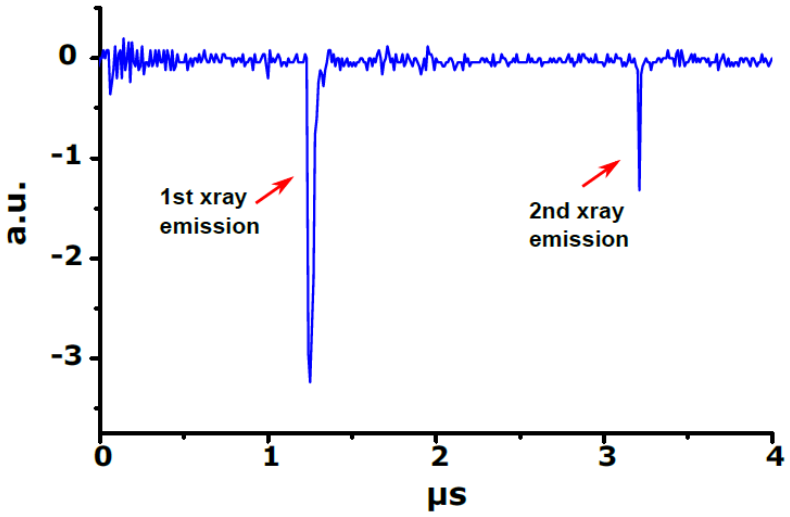

Figure 16: Double x-ray signal emitted from one discharge in the PF device.

3.2.1.2 TLD 100

TLD 100 dosimeters are used to characterize the x-ray emission of the PF2kJ. They are thermoluminescent dosimeters from Harshaw. Their dimensions are 3.1 mm x 3.1 mm x 0.89 mm and their composition is indicated in Table 3 from the section 3.2.1.2.

The TLDs are carefully handled by using tweezers in order to avoid dirt or grease on their surfaces which can affect dosimeter response. They are stored in a plastic case, when they are not being used. This TLD holder is displayed in Figure 17. Letters and numbers have been written in this plastic case for TLD identification. The annealing

and readout procedures are carried out at the dosimetry laboratory at PUC. The ovens used for annealing procedures are: Thermolyne, type 1300 is used to reach 400°C and a JOUAN oven, B1 serie, which is operated at a fixed temperature of 100°C. The TLDs are read by using a Harshaw TLD reader, model 3500, using the WinREMS software to save the signal data.

The glow curves of these LiFMg dosimeters irradiated with nanosecond x-ray pulses from a plasma focus device and from other x-ray source are analysed assuming first order TL kinetics (i.e., assuming dose as proportional to the glow curve integral).

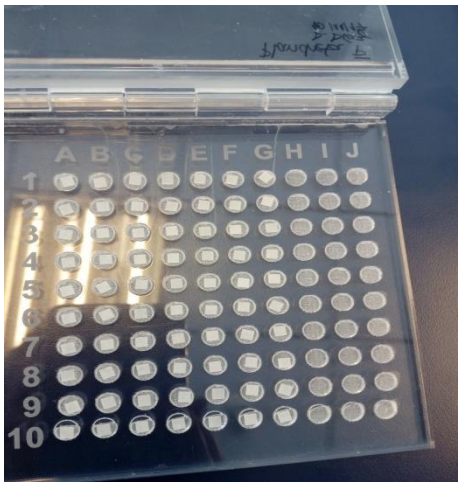

Figure 17: Plastic case for saving and identifying the TLDs.

The annealing cycle and readout of TLD100 dosimeters are specified in [55]. Prior to the irradiation, an 1 hour annealing is applied to the TLDs in an oven at 400 ± 2°C followed by 3 hours at 100 ± 2 °C. After that, they are placed in a petri dish over two metallic bars for 15 min to cool down. TLDs are ready to use 24hr after this annealing. After irradiation, the annealing procedure for pre-readout consist in 10min at 100°C and then TLDs are placed over the metallic bars for 15 min to cool down.

The readout heating is defined from 100°C to 300°C with 10°C/s ramp rate for all TLD 100 type. The dosimeters are placed manually one by one in the reader. Then, the reading values are exported for later analysis. This procedure is repeated every time the dosimeters are used.

Prior to the measurements, intrinsic sensitivity analysis and selection of the TLDs are also required. For that, the entire batch is exposed to similar radiation conditions and the differences are set. Two TLD 100 batches were irradiated with 1Gy in a 6MV clinical photon beam at a distance of the source of 100 cm, using the LINAC from Cancer Center of Pontifical Catholic University of Chile (PUC). The dosimeters are placed between two blocks of water equivalent material, at 5cm depth. The selection process was repeated over time twice, but the last time using a ^{137}Cs source (0.662 MV) from CCHEN in other geometry conditions, also ensuring a homogeneous exposition for all the dosimeters. Intrinsic sensitivity factors were determined on each irradiation for each individual dosimeter. Based on this factor value the selection of the dosimeters was made. A 5% deviation from mean signal was established as selection threshold. An interbatch factor is also determined due to two different TLD batches are used.

3.2.1.3 Radiochromic films

The radiochromic film used in this work is GafChromic EBT2 films from Lot#07301303. The EBT2 films are made by combining a clear, polyester over-laminate with an active film coating. The substrate of the active film is 175 micron of polyester which is coated with an active layer film of 30 microns thickness, over which a topcoat of 5 microns is applied. The over-laminate of 50 micron of polyester, with approximately 25 microns of pressure-sensitive adhesive, is bonded to the coated side of the active film. This non symmetric layer configuration introduces an orientation dependent effect, yielding response deviations for the same scanning orientation when different sides of the film are facing the scanner [67]. The configuration of EBT2 is shown in Figure 18**.**

Prior to irradiation, the films are scanned three times each one by using an EPSON Expression 11000XL scanner with a resolution of 150 dpi (dots per inch). Approximately 24 hours after exposition, the irradiated films are scanned keeping the same position and the same orientation as the previous time (see section of radiochromic films, subsection 2.3.4) by using a paper frame over the scan. The films are analyzed by using ImageJ software. Regarding the film handling, care is taken to manipulate it by its edges and to avoid the light exposure.

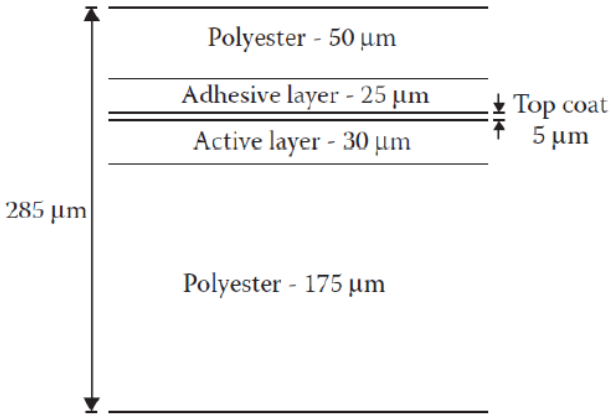

Figure 18: Configuration of GAFCHROMIC EBT2 Dosimetry Film **[67]**.

Since EBT2 film is used to measure the relative spatial distribution of the x-ray emission generated by a PF device, a dose calibration is not required.

3.2.1.4 Ionization chamber (IC)

An IC Farmer-type, FC65-G model, plus a Dose-1 electrometer, both from IBA, are also used for x-ray measurements. This IC has a sensitivity of 21 x 10^{-9} C/Gy in a radiation quality range of 1.3 MeV to 50 MV. A digital barometer/thermometer, Model DBT-100 from CNMC is also used in order to correct the chamber reading by temperature and pressure (see section 2.3.3.1). Prior to every measurement, it was required to set the chamber bias voltage at +300V.

3.2.2 Measurements

3.2.2.1 Pressure efficiency for X-ray emission

This study is intended to establish the pressure that maximizes the x-ray emission. For that, discharges are performed in Hydrogen at pressures from 3 to 12 mbar. Twenty shots are delivered at every different pressure.

The TLD100 are placed in a holder. It is composed by a Petri dish plus foam inside of it. The dimensions of the dish are, one centimetre high, 3.5 cm diameter and 2 mm thick at its base. The foam has 21 holes for holding the dosimeters. They are equally spaced with an inter center distance of 0.65 cm and labelled as shown in Figure 19. On top of the TLDs and inside the Petri dish, a circular foam is placed so that the dosimeters remain fixed, because when this arrangement is placed on the plastic window of the device, the shock waves that are produced in the pinch stage are transmitted beyond the window and the dosimeters may be pushed upwards. This holder will be called *Holder 1* to reference to it in a shorter way in the future. Reference marks are made in the Petri dish (arrow mark) and also in the plasma focus so that they would match. In this way, the setup becomes easier and less error-prone in positioning.

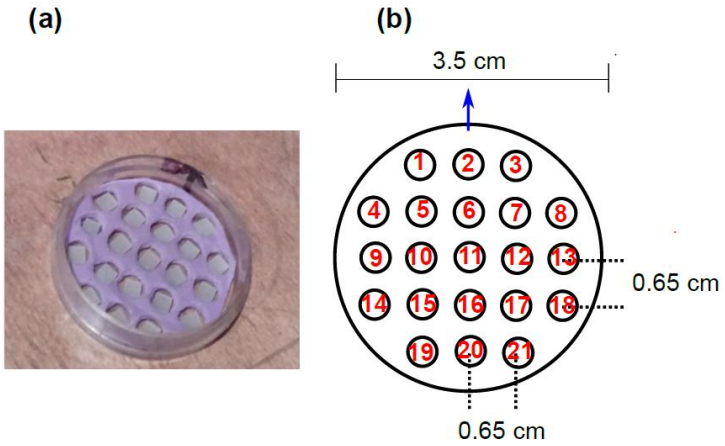

Figure 19: (a) Petri dish plus foam with holes for holding the TLD100. The black arrow used as reference mark is also shown (b) Position label and blue arrow depicting the reference marks used for the setup. The holder dimensions are indicated.

In order to carry out the study, five TLD100 in the central positions (6, 10, 11, 12, 16 array positions in Figure 19 (b)) are placed in the Holder 1 for each PF2kJ operating pressure. The holder is situated over the exit plastic window of the PF2kJ device. This setup is shown in Figure 20. The average and standard deviation from the signal in the five TLDs are calculated. The area under curve of the PMT signal is also determined.

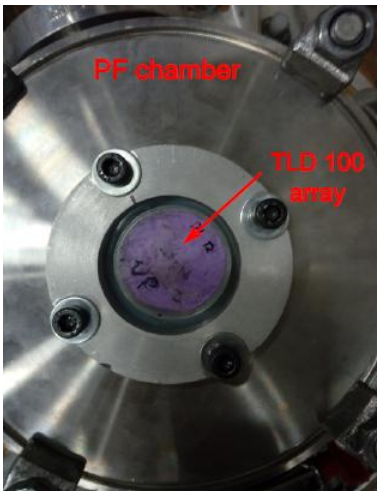

Figure 20: TLD100 array is placed on the plastic window to perform the x-ray measurements.

3.2.2.2 Device warming

Once the pressure that maximizes the x-ray emission is set, a device warming protocol is required in order to ensure that most of the discharges emit x-rays which can be detected by the PMT.

Initially, the device is warmed by performing discharges at 20 mbar. A good pinch formation is observed when a dip in the current derivative from the Rogowski coil appears at this higher pressure. Once this happens, test discharges are performed at the pressure that maximizes the x-ray or neutron emission. The number of shots that is delivered at each pressure is not a set number. This first warming will be called *Warming 1* in order to reference next. Then, a warming protocol is practiced, since there is evidence of the low reproducibility of the shot to shot emission. This warming protocol set the number of shots at 20 mbar at 40 shots that ensure the pinch formation and 10 shots for pressure that maximize the emission. This protocol will be called *Warming 2.*

3.2.2.3 Output linearity study

The output linearity is studied by using TLD 100 in series of 25, 50 and 100 discharges. The discharges taken into account are those that emit x-rays based on the observation of PMT signal. Each series is repeated three times. 21 TLD100 are

placed in the Holder 1 for each series. This experimental setup is shown in the Figure 20. The device is warmed by using the Warming 1 method.

The output linearity study is also performed by using the ionization chamber. For this, a total of 175 shots are delivered in series of 25 shots. The IC is placed at 0.8 cm from the metallic ring (2.3 cm from the plastic window) by using a holder shown later in the Figure 23. The Warming 2 protocol is used for warming.

3.2.2.4 Spatial distribution study

This study intends to determine how the x-ray emission intensity is distributed relative to the central axis of the window. The determination of this spatial distribution is based on measurements using TLD 100 and EBT2 films and no dose calibration is needed.

For the TLDs, the distribution is represented by horizontal (H) and vertical (V) profiles shown in Figure 21. The orientations of these profiles are indicated with blue and green arrows respectively. The coordinate system is also shown in purple and the spatial dimensions of the TLD array have already been indicated in Figure 19 (b). The array is placed centered on the plastic window of PF2kJ. Three series of 25, 50 and 100 shots are delivered with device previously warmed by using Warming 1.

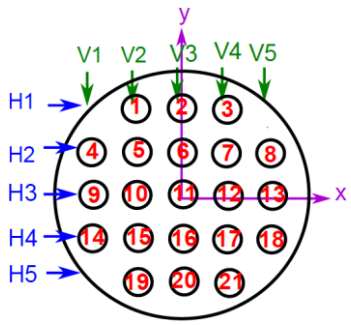

Figure 21: Schematic representation of the positions and the horizontal (H) and vertical (V) profiles of TLD100 dosimeters that are chosen in order to measure the spatial distribution of the x-ray emission.

A radiochromic film of 7 x 5.5 cm^2 is placed at 1.5 cm from the plastic window and 50 discharges are delivered. The device is previously warmed by the Warming 2 method. Gray values of ROIs are obtained and then, the netOD is calculated. The ROIs

selection is shown in Figure 22. They are chosen so that they can be compared with the spatial distribution obtained by TLD100 measurements. In order to match the two spatial distribution obtained by these two detectors, the emission divergence is considered. Horizontal (H) and vertical (V) profiles are indicated in Figure 22 and the TLD 100 positions are also indicated but not at scale.

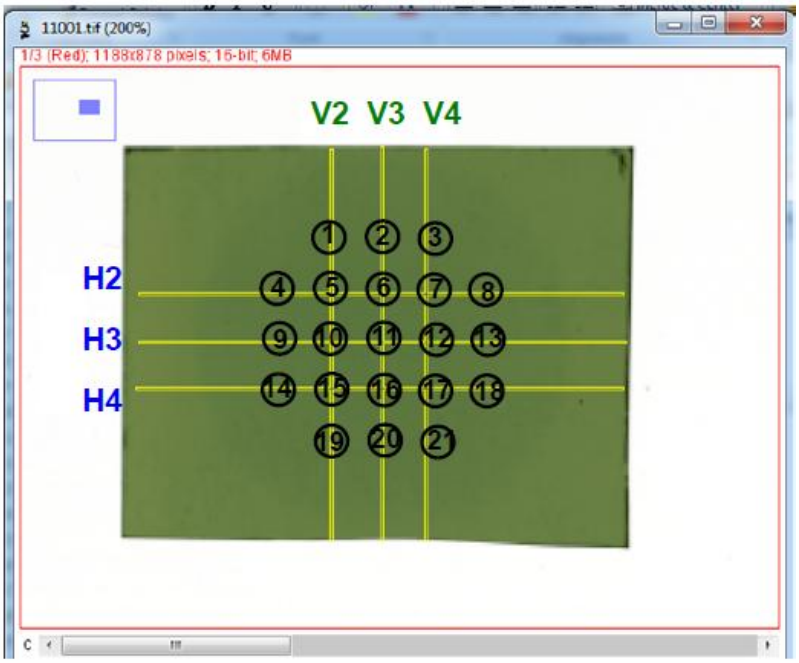

Figure 22: The yellow lines correspond to ROIs selected in ImageJ software.

3.2.2.5 Virtual source study

Based on the expression of the inverse squared law, it was shown that the terms can be arranged so that a linear equation arises (see equation (7)). From this equation, the dependent variable corresponds to $\sqrt{I(L_0)}/\sqrt{I(L)}$, the independent variable is the distance, the slope is $1/(L_0 + S_V)$ and the intercept is $S_V/(L_0 + S_V)$. Here, the intercept with the abscissa axis yields the shift of virtual source from the reference distance L_0 outside of the PF chamber and it is calculated as the negative value of the ratio between the intercept with the ordinate axis and the slope. These values are calculated by using OriginPro 8 program. In the case of PF device, if the virtual source is Sv>0, it means that the physical source is outside the chamber of PF2kJ device, but if Sv<0, the physical source will be inside it.

The x-ray emission from PF2kJ was measured at different distances from the plastic window ($I(L)$) by using the ionization chamber (Measurement 1) and the TLDs100 (Measurement 2).

For performing the Measurement 1, The IC is placed at 2.3 cm, 6.5 cm, 11.5 cm, 16.5 cm, 25.8 cm, 36.5 cm and 48 cm by using a holder. Two series of 20 discharges are performed per each distance consecutively.

For performing the Measurement 2, groups of four TLD100 are placed at 2.5 cm, 6.8 cm, 11.5 cm, 16.5 cm, 21.5 cm, 25.7 cm, 36.5 cm and 47.5 cm. They are put inside a Petri dish with foam in the base. The foam has a square hold at the center where the four TLDs can be as close together as possible. The Petri dish is held in the air by the same metallic holder used to the IC measurements, as shown in Figure 23 (TLD array 1). Series of 25 discharges are performed per distance.

In order to correct the emission variation related to the change of distance from output variations arising from the device instability, another array of four TL dosimeters (TLD array 2 in Figure 23) is placed at the exit of the window of PF2kJ. This signal is used to correct TLD measurements, while the area under the curve of the PMT signal is used to correct IC measurements. The dosimeters of this second TLD100 array are changed every time that a new measurement is performed and they are placed together on the center of a paper holder at a 1.5 cm of distance from the plastic window.

In a general, if R_i is the mean readout from the detector that measure the x-ray emission variation of interest; M_i is the mean readout from the output monitoring detector (TLD or PMT) and M_0 is the monitoring reference value on which the output correction is based, then, an output correction factor can be determined by:

$$F_i = \frac{M_0}{M_i} \tag{8}$$

The i index refers to the different experimental setup performed related to the same experimental study. Then, R_i values are corrected by multiplying it by this factor.

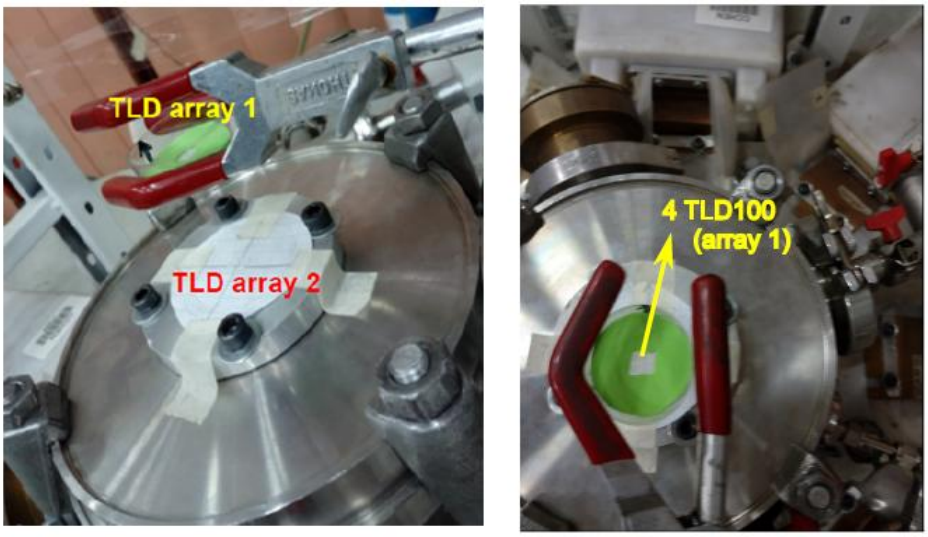

Figure 23: Experimental setup for determining the x-ray emission source. Two TLD100 arrays are used; one measures the variation of the emission with the distance (array 1), and the other measures the output variation of the emission from the device (array 2).

3.2.2.6 HVL and effective energy study

Transmission measurements of the x-ray emission through Aluminium foils of different thicknesses are performed in order to determine HVL and the effective energy of the emission. These measurements were carried out by using two different detectors: an array of four TLDs100 and an IC, which were placed at 4 cm and 2.5 cm from the plastic window, respectively. The first measurement is made with no attenuator material between the x-ray source and the detector, and then measurements are made with successively thicker attenuating Aluminium material. The thicknesses used ranged from 0.1 to 0.7 mm in steps of 0.1 mm when TLDs are used, and 0.1 to 0.4 mm in steps of 0.1 mm in the other case. The Aluminium foils are from ESPI Metals, having dimensions of 0.04'' x 10 cm x 10 cm and others of 0.008'' x 10 cm x 10 cm, with a purity of 3N (99.9%). These filters are placed over the PF device metallic ring at 2 cm from the plastic window. 20 discharges are performed per each thickness including the zero thickness; however two series of 20 discharges per filter thickness are performed in case of IC measurements.

In order to correct for the output variation, four TLDs are placed at 1.5 cm from the plastic window for monitoring. This experimental setup is shown in the Figure 24.

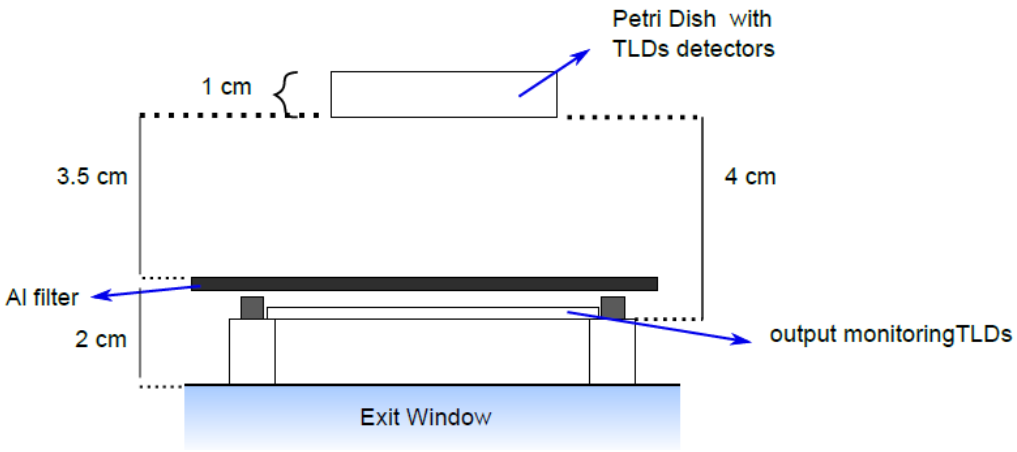

Figure 24: Experimental setup to measure the transmission values for different Aluminium foil thicknesses.

Once the transmission values are determined, the logarithm of these values against the thicknesses are plotted in order to determine the linear attenuation coefficient (and effective energy) from the slope of the curve at a thickness corresponding to the HVL. The data for interpolation for estimation of effective energy are taken from [72].

3.2.2.7 Radiation protection

In order to monitor the operator personnel ionizing photon radiation exposure due to the PF2kJ device, eight TLD100 are placed surrounding the device during 70 days approximately. Two dosimeters are placed in each position as shown in the Figure 25 . After the period of time, they are read and the mean charge is obtained for each position.

A calibration is needed in order to translate the TLD signal into values of personal dose equivalent $H_p(10)$ for the dosimeters placed around the device and also for those placed directly on the chamber plastic window. The calibration is performed at the Laboratory of Metrology of Radiations Ionizing (LMRI) from CCHEN. This is a secondary standard dosimetry laboratory.

The calibration is performed at different dose equivalent values by using a source with the lowest energy available at CCHEN facility since it is the most similar to that expected from the x-ray source of the plasma focus device. This calibration source has an effective energy of 15 keV (32 kV). Four TLDs100 are exposed at different

personal dose equivalent values placed at the surface of equivalent tissue ICRU phantom (30 x 30 x 15 cm^3), where a previously calibrated ionization chamber (NPL 303) gives the conversion to $H_p(10)$ values. The dose values were reported with a combined uncertainty of 5.7% (1.5% for type A uncertainties and 5.5% for type B uncertainties).

In addition, the correction of theTLD100 readout values after the calibration exposure due to the energy dependence of the response of the TLD100 (the effective energy used at calibration process is different from the x-ray emission from PF2kJ) can be estimated based on the Figure 9 from the data in the reference [60], where the normalized response values (normalized to ^{60}Co) between 1 and 1.4 are reported for the TLD100 detectors for x-ray energy between 10 and 150 keV with a local maximum around 30 keV.

Once the personal dose equivalent values are gotten before calibration and the correction due to TLD 100 energy response variation is taken into account, it can be assessed if the exposure level is within the dose constraints that ICRP recommends regarding occupational exposure in planned exposure situations.

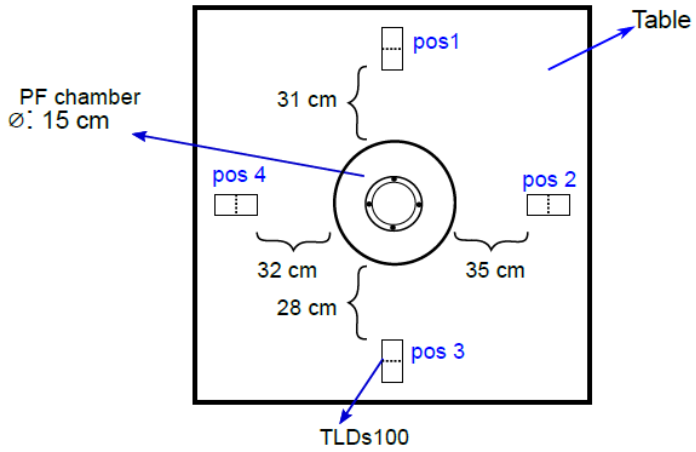

Figure 25: Top view of the PF2kJ device. The positions (1 to 4) of the TLDs100 around the device are indicated.

3.3 Neutron emission characterization

Two neutron detectors are used in this work in order to detect the neutrons generated by a plasma focus device when the filling gas is Deuterium: a ^3He

proportional counter and pairs of TLD 600 and 700. First, they will be described and specifications of interest will be detailed. Then, the different studies performed regarding the neutron emission of the PF2kJ device are described.

3.3.1 Neutron detectors

3.3.1.1 ^{3}He proportional counter

Since ^{3}He neutron detector shows a high sensitivity to thermal neutrons and the emitted neutrons from plasma focus had been previously estimated to be about 2.45 MeV, a moderator is included in the detection system in order to increase the detector efficiency. A block of paraffin of 45x15x15 cm^{3} dimensions is used with this purpose. The system is covered with a cadmium sheet to minimize the thermal neutron background and encapsulated in an aluminium box. The proportional counter plus the system moderation and Al box is named as ^{3}He-206. The analogue signal corresponding to the current generated in the ^{3}He tube is processed through a Camberra preamplifier (model 2006) whose output is directly connected to a digital phosphor oscilloscope, TDS5104B.

A neutron signal from the ^{3}He-206 detector system is shown in Figure 26. The neutron yield is quantified by direct time-integration of the signal extracted from the oscilloscope. In [77] it is established a method that correlates the area under curve of the ^{3}He signal with neutron yield. The entire detection system was previously calibrated in a ^{241}Am-Be neutron source in a specific geometry in order to obtain the neutron yield value for the PF2kJ device. This neutron source is chosen since it has a similar neutron spectrum centered around 3 MeV close to the energy of the neutrons in the PF device. This calibration stage was not performed in this thesis. However the general procedure is described in [78] and [77]. For signal integration, a routine in Python was used and it was provided by Jalaj Jain, who is an investigator at CCHEN. Prior to every measurement session using this system, the background neutron signal must be determined.

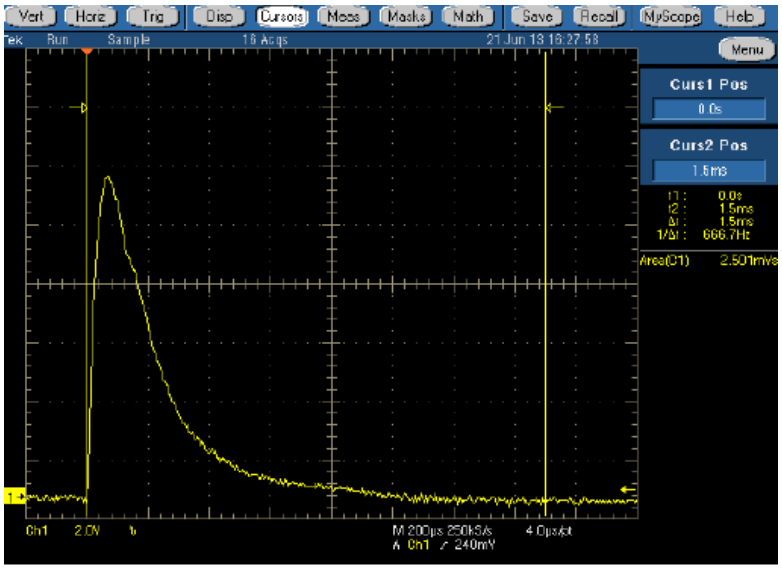

Figure 26: Signal of ^{3}He detector when neutrons are present. The area under the curve is proportional to the neutron yield.

The ^{3}He detector is placed at 130 centimetres in front of the lateral plastic window of the PF2kJ chamber for all the measurements performed in this work.

3.3.1.2 TLD600-700 dosimeters

TLD 600 and 700 from Harshaw are used in order to quantify the x-ray and neutron emission from the mixed source of the device. The dimensions, handling, pre-annealing and annealing protocols are the same as for TLDs100. Their compositions are indicated in Table 3 from the section 3.2.1.2. The readout heating is defined from 100°C to 350°C with 7°C/s ramp rate. The dosimeters are placed manually one by one in the same reader that was used for TLD 100 and the readout values are exported for later analysis.

Before measuring the emission in PF2kJ, TLD 600 and TLD 700 are irradiated in a ^{137}Cs source (0.662 MeV) to determine their intrinsic sensitivity factor to photon radiation and to select them based on the 5% of deviation from the mean value. Then, the dosimeters are ready for their use.

Then, the dosimeters are also calibrated in terms of personal dose equivalent $H_p(10)$ in order to convert the charge values into dose values. For this, TLD 600 are irradiated at different dose equivalent $H_p(10)$ in the ^{241}Am-Be source (fast neutron

source) and TLD 700 are irradiated at different dose equivalent $H_p(10)$ in the ^{137}Cs source, with a reported combined uncertainty of 5.7% in dose values.

The irradiations mentioned above are carried out at the Laboratory of Metrology of Ionizing Radiations (LMRI) of CCHEN.

3.3.2 Neutron measurements

The first part of the study is intended to determine the pressure that maximizes the neutron emission and the second part of the study is intended to measure pulsed neutron emission by using pairs of TLD600 and 700 at different setup configurations.

3.3.2.1 Pressure efficiency for neutron emission

Based on the ^3He detector system, the pressure at which the neutron emission is the highest is determined. For that, discharges are performed in Deuterium (D_2) at pressures values from 10 to 3 mbar in decrements of one mbar. Thirty shots are delivered at every different pressure. Then, the same measurement is repeated, this time going up in pressure value, in order to evaluate possible systematic differences due to the accumulation of discharges.

3.3.2.2 Output linearity

Different experimental setups are performed in order to determine the best experimental configuration to detect neutron signal in TLD600-700. Since the TLD600 dosimeters respond mainly to thermal neutrons, different thicknesses of polyethylene are used in order to identify the thickness that maximizes their responses. The response varying the number of discharges in D_2 is also studied. All the measurements are performed by ^3He monitoring of the neutron emission, with this detector placed in front of the lateral window of the PF2kJ chamber at 130 cm. The pairs of TLDs 600-700 are placed on the plastic window that is on the top of the chamber (axis direction). In order to estimate the neutron emission in the axis direction, it is required to take into account the anisotropy of the neutron emission (Y(0°)/Y(90°)), since the yield obtained comes from the ^3He detector that is placed at

the side of the chamber. This anisotropy is not measured, but it is estimated by data in the literature. It can be seen that the anisotropy factor ranges from 1.25 to 1.5 based on the values given for several devices in Table 2. In this way, the neutron yield in the axis direction could be estimated from the measurements at the side of the chamber by using ^{3}He and applying the anisotropy factor.

3.3.2.2.1 TLD response varying the number of discharges

In the first attempt to measure neutron emission by using pairs of TLD600 and 700, a 4 cm polyethylene moderator is placed on the metallic ring surrounding the plastic window of the device. Three pairs of TLDs are placed in a plastic (polyethylene) holder that it is put on the moderator. Then, the TLD array is at 7 cm from the exit window. The experimental setup and the TLD-holder are shown in the Figure 27. The total thickness of the moderator is 5 cm since the TLD holder has 1 cm thickness. The 5 cm thickness of moderator is suggested by personnel (Mr. Ricardo Ávila) of the dosimetry laboratory at CCHEN, a robust signal in TLD 600 has been observed when they are irradiated in a ^{241}Am-Be source by using around this filter to thermalize the neutrons. Finally, a polyethylene slab of 1 cm is placed on the TLD array to provide backscatter. 150 and 300 discharges are performed in D_2 at 6 mbar. Then, the thickness moderator is fixed and the number of discharges varies in order to determine the necessary number of discharges to see a signal in TLD dosimeters.

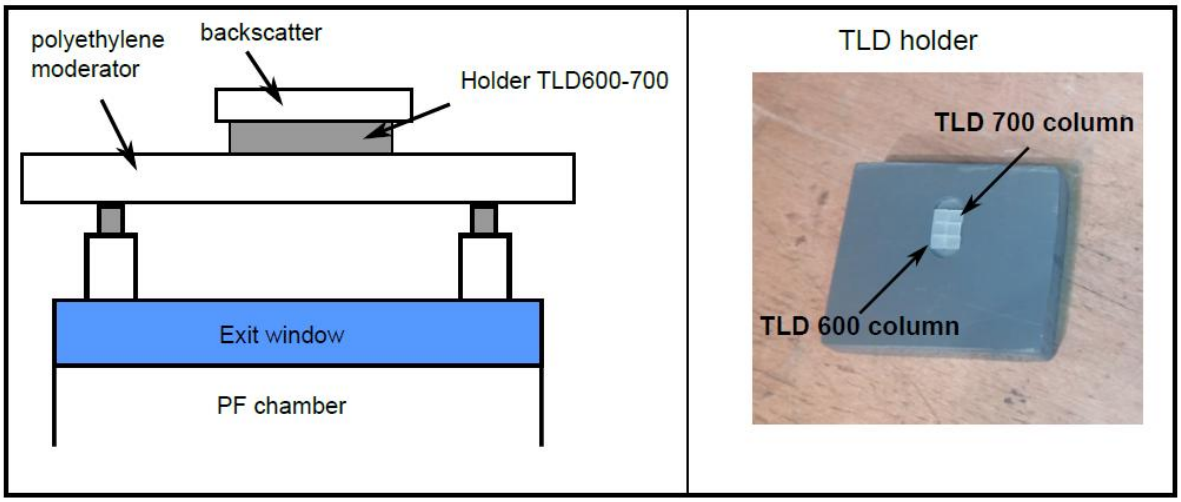

Figure 27: Experimental setting to measure neutron emission by using pairs of TLD600 and 700 when a 5cm moderator is used. The holder used for the dosimeters is shown on the right picture.

3.3.2.2.2 TLD response varying the moderator thickness

Three different moderator thicknesses are used at the same time to determine which one maximizes the response in the TLD600 regarding neutron emission. The experimental setup is shown in Figure 28. It is a TLD-moderator sandwich setup, and it will be described from the bottom up. First, three TLD600-700 pairs (array 1) are placed at 2 cm from the plastic window that is on the top of the chamber, a 4 cm moderator is placed on them. Then three more pairs are placed on this moderator (array 2). Finally, a 1cm moderator on top of the array 2, another three TLD pairs and a polyethylene slab as backscatter are placed in the order mentioned. The arrays 1 and 3 are placed in foam of approximately 6mm thick with holes to put the dosimeters. The array 2 is placed in the holder used before (see Figure 27), and this holder acts also as moderator for the array 3.

The total neutron yield is determined based on the ^{3}He signal being estimated at axis direction by using the anisotropy factor from literature.

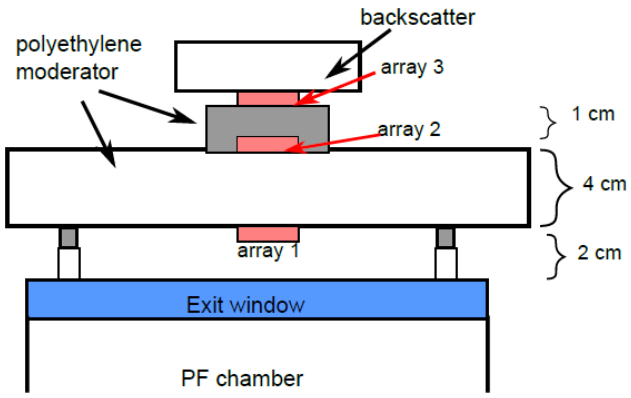

Figure 28: Experimental setup by using no moderator, 4 cm moderator and 5 cm moderator at the same time when 450 shots are delivered. Three arrays of three TLD 600-700 pairs are placed between them as indicated in the figure**.**

4. Results and Discussion

4.1 Dosimeters

4.1.1 Intrinsic sensitivity factor (ISF)

4.1.1.1 TLD 100

A histogram of the ISFs for the TLDs 100 used during all the measuring period are shown in Figure 29. Three selection stages during TLD usage are shown at different colours. The first two selections are performed by using a 6MV source of a LINAC and the last selection was performed by using a ^{137}Cs source. The mean of ISF was 1.004±0.06 considering the three selections, with a minimum value of 0.8 and a maximum of 1.2. The dosimeters out of the threshold selection were discarded in each selection stage. The percentage of dosimeters selected are 87%, 75%, and 63%, corresponding to the 1st, 2nd and 3rd selection respectively. It can be seen that the number of dosimeters decrease while the period of usage increases.

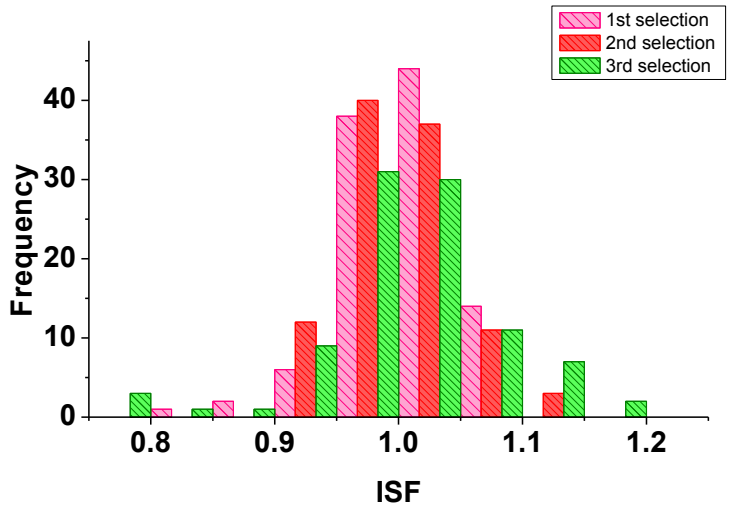

Figure 29: Histogram of the ISF values for TLD100 dosimeters used during all the measuring period.

4.1.1.2 TLD 600 and TLD 700

The dosimeters are irradiated at 88mGy in a ^{137}Cs photon source of 662keV energy to determine their individual intrinsic sensitivity to photon radiation and select them. The ISF to photon radiation are calculated for both dosimeter types and their values are shown in Figure 30. It can be notice that two TLD 700 are outliers.

It can be observed that the photon responses are similar for the two type of dosimeters, since the ratio between the mean outputs of dosimeters TLD 600 and TLD 700 results in 0.99±0.04. This result is in agreement with the literature [79]. A

mean value of 0.99±0.03 is obtained for ISFs values, with minimum and maximum values of 0.92 and 1.04 respectively.

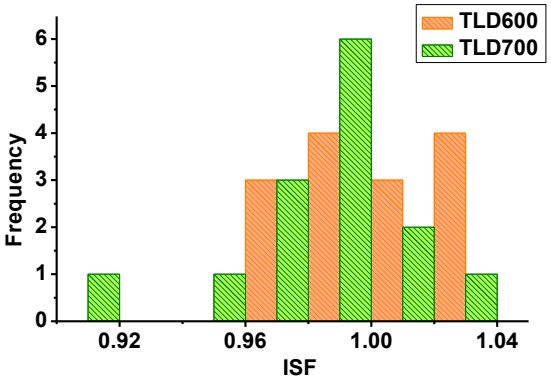

Figure 30: Histogram of the ISFs for TLD 600 and TLD 700 dosimeters.

4.1.2 Calibration factor (CF)

4.1.2.1 TLD 100

In order to translate the light readout values of the TLD100 into $H_p(10)$ values, the calibration factor is determined by plotting the $H_p(10)$ values reported by CCHEN when a calibration source of 32kV (effective energy of 15keV) is used, against the outputs of the TLDs100 exposed in this calibration process. The calibration curve is shown in Figure 31 and Table 4 shows the values plotted. The calibration factor is determined from the slope giving a value of 0.167 ± 0.003 mSv/nC.

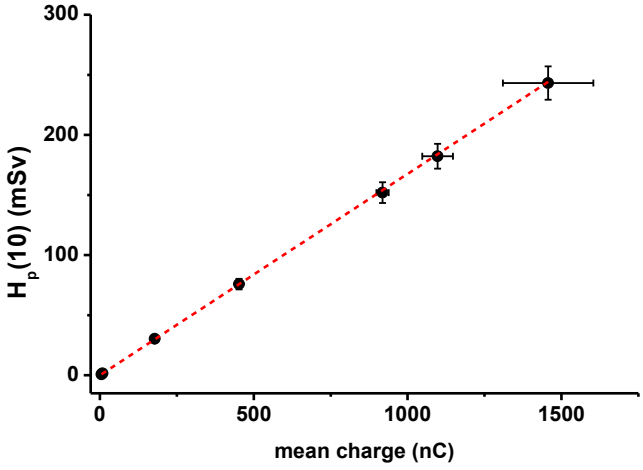

Figure 31: Calibration curve for TLD100 in terms of $H_p(10)$. The effective energy of the calibration source is 15 keV.

Table 4: $H_p(10)$ values and the corresponding mean charge collected for different expositions used to determine the calibration factor at an effective energy of calibration of 15keV

$H_P(10)$ (mSv)	Mean charge (nC)
243.19 ± 13.86	1541.35 ± 9.44
182.24 ± 10.39	1097.36 ± 49.90
151.99 ± 8.66	918.36 ± 20.05
75.84 ± 4.32	452.39 ± 5.61
30.4 ± 1.73	178.46 ± 1.48
1.56 ± 0.09	4.99 ± 0.07

4.1.2.2 TLD 600 and TLD 700

A calibration factor (CF) is determined for both types of dosimeters. In order to determine it, TLD 600 are irradiated in $H_p(10)$ conditions, at different personal dose equivalent values by using a ^{241}Am-Be fast neutron source as well as TLD 700 are irradiated by using a ^{137}Cs photon source. The mean charge obtained from the TLDs readings corresponding to a $H_p(10)$ value are shown in Table 5 for both types of dosimeters.

Table 5: Mean charge from TLDs 700 and TLDs 600 when they are irradiated at different personal dose equivalent values. The corresponding plot are shown in Figure 32(a) and Figure 32(b) respectively.

TLD600		TLD 700	
$H_p(10)$ (mSv)	Mean charge (nC)	$H_p(10)$ (mSv)	Mean charge (nC)
4.65±0.27	34.65±0.58	0.53±0.03	6.76±0.23
2.29±0.13	15.55±0.52	1.06±0.06	15.0±2.16
1.38±0.08	9.41±0.96	2.11±0.12	27.5±2.98
0.56±0.03	5.53±0.26	5.29±0.30	54.78±0.96

Since Am-Be source emits also gamma radiation, it is needed to substract the contribution in the response of TLD 600. It is estimated a 24% of gamma contribution in TLD 600 readout when TLD 600 and TLD 700 are irradiated together in this source at 1.13 mSv and placed at 170 cm. This is a rough estimation by simple substraction of the TLD 700 signal from the TLD 600 signal, since the gamma contribution varies while distance from the source varies. Then, the CF is determined by the slope from the corresponding curve, obtaining a CF of (0.20 ± 0.01) mSv/nC for TLD 600 and (0.08 ± 0.004) mSv/nC for TLD 700.

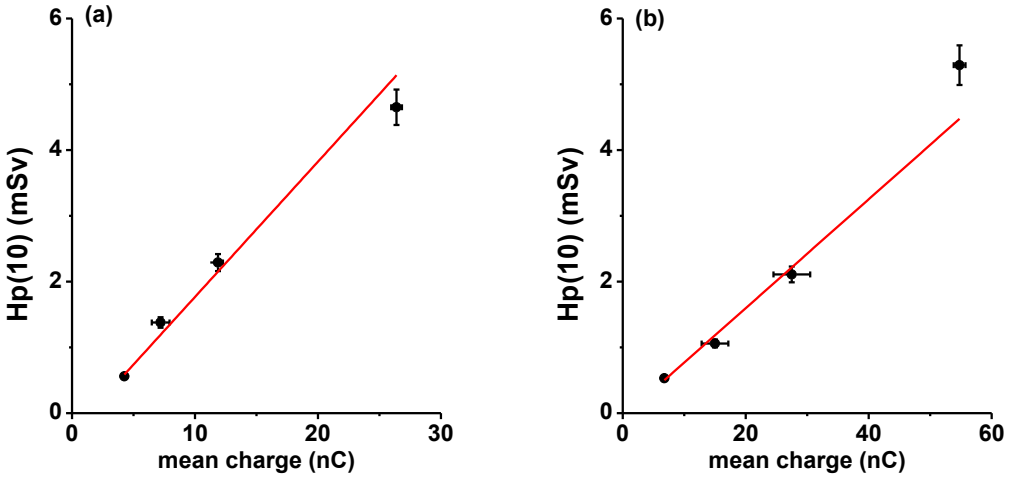

Figure 32: Calibration curves for **(a)** TLD 600 and **(b)** TLD 700.

4.2 X-ray emission

4.2.1 X-ray emission efficiency as a function of pressure variations

The pressure at which the greatest charge value is observed in TL signal and the value of the area under the curve of the PMT signal are studied. Both values were calculated as explained in sections 3.2.1.1and 3.2.1.2.

The number of shots with x-ray emission based on the PMT signal, divided by the total number of discharges delivered is displayed in Figure 33(a) showing that the gas pressure has a significant effect on the x-ray emission. It is observed that the highest number of shots with x-ray emission occurs at 7 mbar of pressure, where the 85% of the total shots emitted x-rays detectable by the PMT. The Figure 33(b) shows

that as expected the sum of the area under curve of PMT signal as the mean charge of the five TLD-100 reach the highest values at 7 mbar. It is established based on this study that the next x-ray emission experiments will be carried out at this gas pressure.

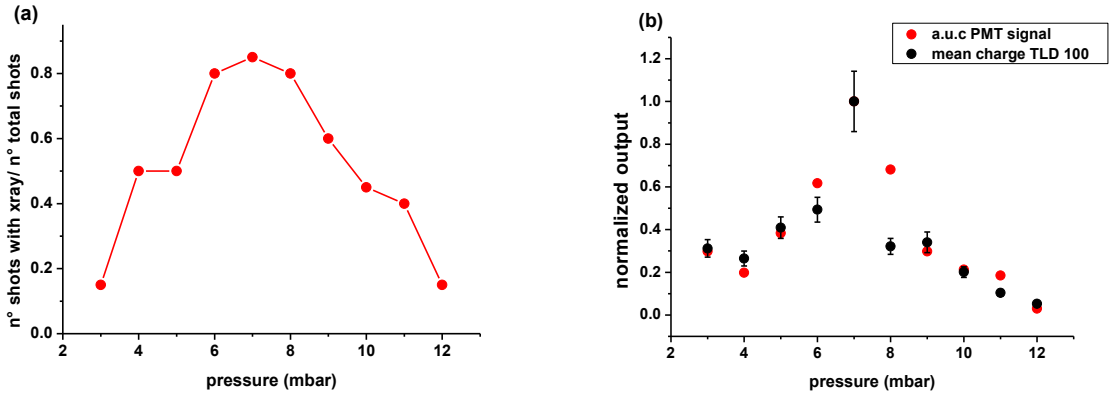

Figure 33: Study of the filling pressure variation to find the optimum x-ray emission. **(a)** Ratio between the number of shots that emitted x-rays and the total number of shots delivered. **(b)** Mean charge from seven TLD 100 (black) and area under curve of the PMT signal (red) when the filling pressure is increased from 3 to 12 mbar.

A difference between the output measured by TLD and PMT can be noticed in the Figure 33(b). This difference is higher at 8 mbar. It is possible that the x-ray spectrum emitted by the PF2kJ device changes with the changes of pressure due to the fact that TLD 100 crystals respond to all gamma energies while PMT only above 100 keV. Nevertheless, there is a good agreement between the responses of the two applied detectors.

It is explained in [80] that the x-ray emission depends on the pressure because the density in the pinched plasma increases when pressure increases from a low value, therefore, the x-ray emission also increases. Nevertheless, beyond a certain pressure the plasma sheath shows instabilities and the time to pinch exceeds the time to maximum current, causing that the maximum compression occurs at lower current reducing the x-ray emission. For that reason, a maximum in the x-ray emission is usually observed, as in this work. The optimum pressure is thus specific for each PF device.

4.2.2 Device warming

In Figure 34 it is plotted consecutively the area under curve (a.u.c.) of the PMT signal for every shot delivered at 7 mbar when the Warming 2 protocol is implemented on two different days. The discharges performed at the warming stage are also included when the filling pressure is 7mbar but not when 20 mbar is used, since in this case, x-ray emission was not detected by the scintillator-PM detector. It can be noticed that the warming process gives a good protocol to ensure that x-ray emission occurs but it does not guarantee that the intensity of the x-ray emission is the same per shot nor per day. Then, it would be necessary to correct for some factor that normalizes the measurements that require quantifying variations that are not related to the device output variations.

This low reproducibility of the emission output of the discharges has been also reported in [34].

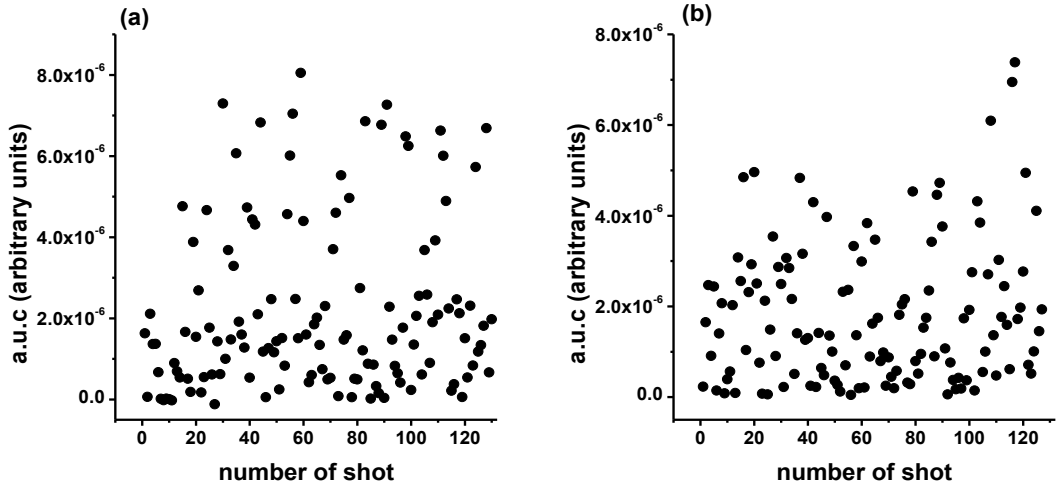

Figure 34: The area under curve from the PMT signal is plotted against the number of shots performed consecutively for several measurements made at different days that corresponds to **(a)** and **(b)**.

4.2.3 Output linearity

This study is performed with the aim to find some relation between the output measured by radiation detectors (TLD100 and ionization chamber) and other parameters such as the number of shots, the number of shots with effective presence of x-ray emission based on PMT signal, or the a.u.c of PMT signal.

First the output variation measured with TLD 100 is studied for different numbers of shots. The mean charge obtained from the five central positions in the array of 21 TLD100 (6, 10, 11 12 and 16 positions) is plotted against the number of shots that emitted x-rays based on the observation of the PMT signal (Figure 35(a)) and against the number of total shots (Figure 35(b)). It can be noticed from the plots that the output measured in charge by the TLDs 100 increases with the number of shots. Nevertheless, there is not a clear linear relation for any of these parameters since the R-squared values are 0.81 and 0.75 respectively.

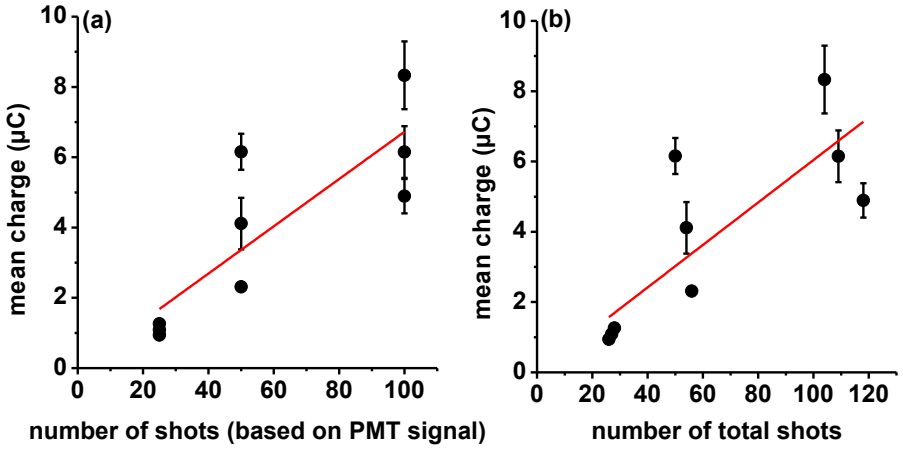

Figure 35: Output of x-ray emission measured by TLD100 for: **(a)** different numbers of shots that emitted x-rays (based on the observation of PMT signal) and **(b)** different numbers of total shots.

The low reproducibility, already found in the study based on the PMT signal, can be also observed using TLDs 100 by considering the data from other days. Figure 36 shows the outputs corresponding to different number of series of 20 total discharges on three different days (black, red and blue colours corresponding to each day). Deviations up to 75% in the discharge series are observed on one day (red colour). Deviations of 10% and 20% correspond to the other days (black and blue

respectively). Therefore, it is needed to relate the output device with another parameter instead of the number of discharges.

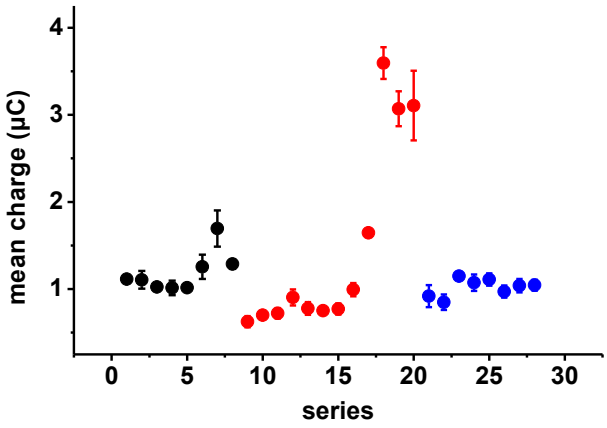

Figure 36: Mean output from TLD 100 when series of 20 discharges are delivered consecutively on different days indicated by the different colours.

If the mean charge is instead plotted versus the sum of the area under curve of the PMT signal, a strong correlation between these two parameters is observed (Figure 37). The error bars in Figure 37 are of the order of 10% and corresponds to standard deviation of the five TLDs 100. Hence, a linear fit with zero intercept was performed where the slope was 3.21×10^{7} nC/Vs ± 5%, with a good correlation coefficient of 0.95.

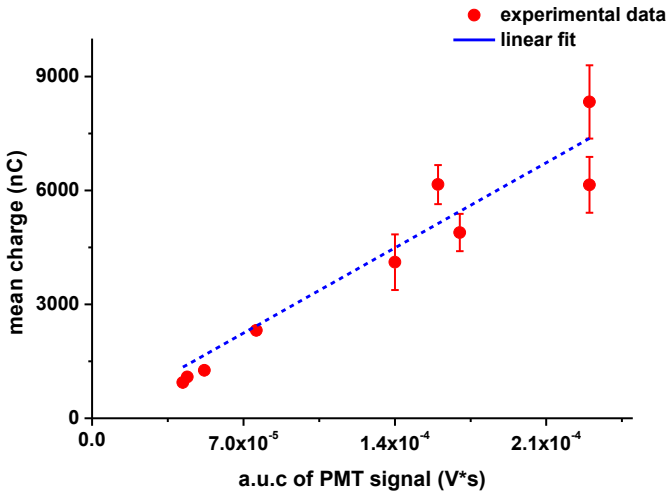

Figure 37: X-ray emission output measured with TLD-100 plotted against the corresponding area under curve of the PMT signal.

The relation between the TLD response and the PMT signal per shot has been studied in [81] by performing the discharges with D_2 as filling gas in a PF device of 2kJ. The PMT amplitude peak and the dose measured with TLDs 200 exhibits a

correlation coefficient of 0.86 (see Figure 38) when the crystals are placed in front of a 5 mm thick glass window outside the discharge chamber. The study performed in [81] and the present study show similar results because the peak and the area under curve in the most PMT signals are proportional in this thesis study since the signal shape is a triangle. Two proportion values can be obtained depending on the amplitude as shown in Figure 39 . The red line shows the tendency of low amplitude signals while blue line shows the tendency of high amplitude signals, however high data dispersion is observed for the two cases.

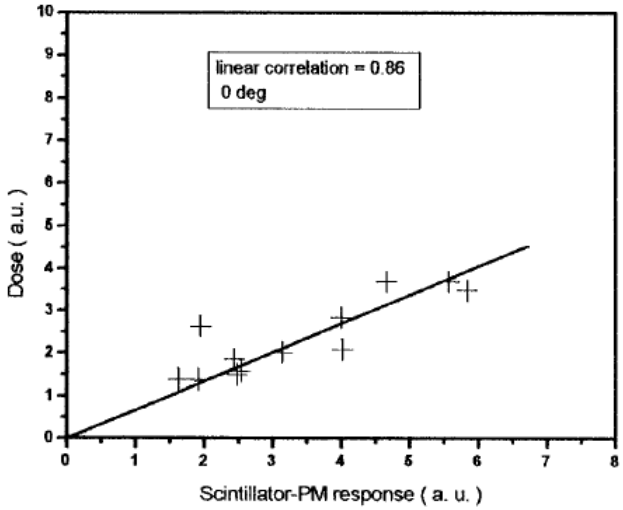

Figure 38: Scintillator-PM detector signal versus TLD 200 response for x-rays from a PF device when the both detectors are placed in front of the glass window outside the device chamber. The values are given in arbitrary units. Figure taken from [81].

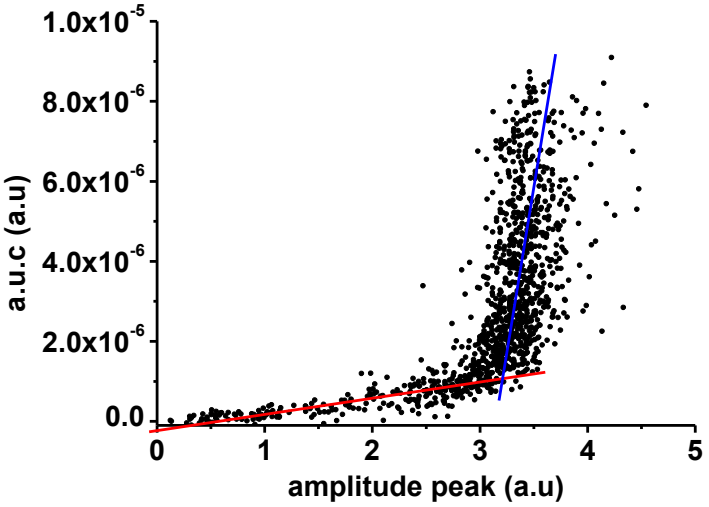

Figure 39: Amplitude of PMT signal against the area under the curve of this signal for different individual discharges.

The output linearity study is also performed by using ionization chamber (IC) radiation detector. The charge collected in five discharges by the ionization chamber

is plotted against the sum of the areas under curve of the corresponding PMT signals in Figure 40. The linear correlation is good (R^2=0.88) although higher dispersion is observed for higher values.

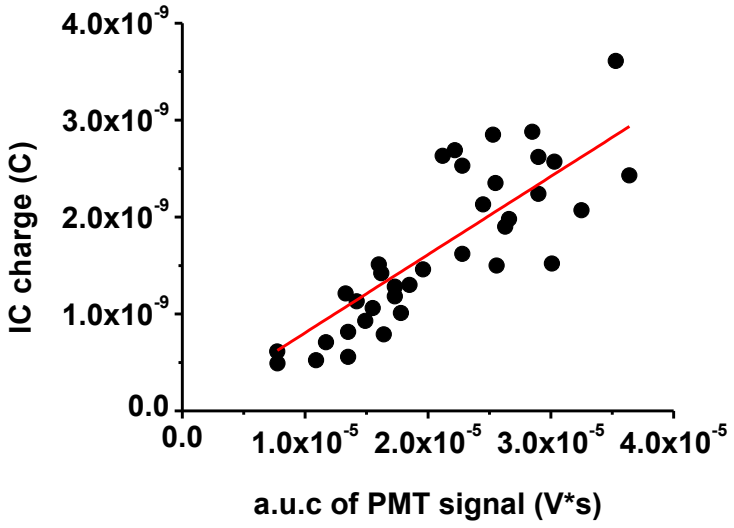

Figure 40: IC output against the PMT output per shot.

A low shot to shot reproducibility is observed from the linear output study of the PF 2kJ device. This behaviour does not allow to establish a linear relation between the output and the number of discharges, while it is possible to do it between the radiation detectors (TLD100 and IC) and the area under the curve of the PMT signal, despite the fact that they have different energy responses (TLD100 and IC respond to a wide range of photon energies and PMT only above 100 keV). Based on this, it can be also said that the x-ray emission spectrum remains similar on average so that this linear relation can be observed.

4.2.4 Spatial distribution

Spatial distribution measured by TLDs 100 was performed. The results are shown in Figure 41 for the horizontal and vertical profiles. Since the charge in every position of the TLD array corresponds to different numbers of discharges, it was required to normalize the charge values by dividing each value by the area under curve of the PMT signal. This correction method was chosen as the previous study concluded that this quantity showed the highest correlation with the detector signal under equal conditions. The error of the position is not depicted but it corresponds to 0.5 mm.

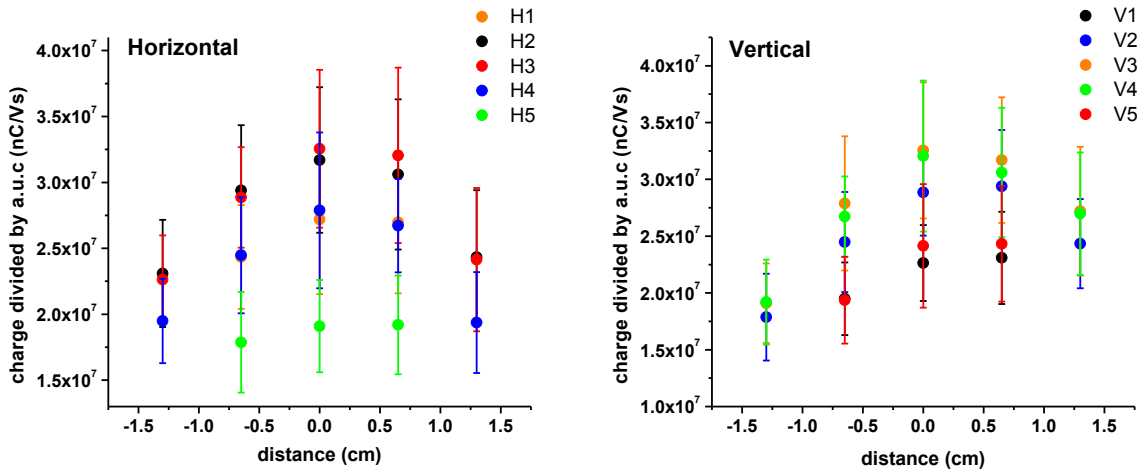

Figure 41: Horizontal and vertical profiles measured by using TLD100 corrected by the a.u.c of the PMT signal to obtain the charge by one shot.

An asymmetric spatial distribution is observed where the central position in the array has the highest output. The intensity of the emission decreases outwards. This decrease is mainly appreciated in the lower part of the arrangement where the intensity is 43% lower compared to the center. The output also decreases on the left side (around 30% less signal). These lower values are noticed at an average distance of 1.5 cm from the central position.

The relative profiles have also been obtained by using EBT2 films being smoothed by the Savitzky-Golay filter method, which performs a local polynomial regression around each point. These smoothed profiles and those measured with TLDs 100 are shown in Figure 42 and Figure 43. The horizontal and vertical profiles are labelled as specified at section 3.2.2.4.

The standard deviation of the spatial distribution measurements performed through radiochromic films (standard deviation not shown in plot) and TLD 100 are 12% and 30% respectively, being higher for TLD100 since this study was performed at several days and then, the output variation associated to the device warming and the low shot to shot reproducibility is present, while the spatial distribution by using EBT2 was performed on the same day and it has its origin from the times the film was scanned. The maximum value is at the center of the all profiles for the two methods,

excepting for H4 and V4. The greatest differences are found in the left part of the all profiles and are bigger for horizontal profiles, reaching up to 20% difference.

FWHM values are calculated for every profile and similar values are obtained. The mean FWHM values are 3.5 ± 0.02 and 4.1 ± 0.1 for vertical and horizontal profiles respectively by using EBT2; and 3.7 ± 0.01 and 3.7 ± 0.3 for those measured with TLD 100. The symmetry is also evaluated for EBT2 relative profiles, by calculating the percentage difference between the areas under the curve of the left/down and right/up side of the profile. This value is -6% approximately for all vertical profiles and 3% up to 6% in the horizontal profiles. Therefore, higher intensities are present on the top right of the emission.

In spite of the measurements were performed different days and thus setup errors may be increased, the agreement in spatial distribution with the two methods are reasonably good, at least they reproduce in similar way the shape of the emission for the most of the profiles (20% maximum difference). Evidence of this is the similarity between the FWHM values obtained by the different methods (10% maximum difference).

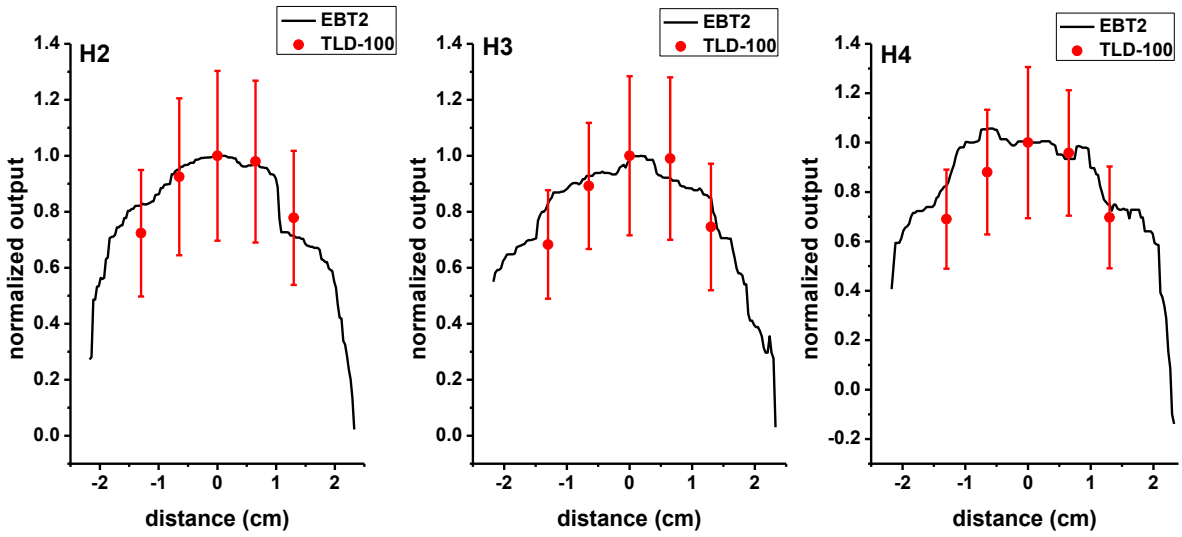

Figure 42: Horizontal profiles from EBT2 radiochromic film measurements. The profiles measured with TLD-100 are also show for comparison.

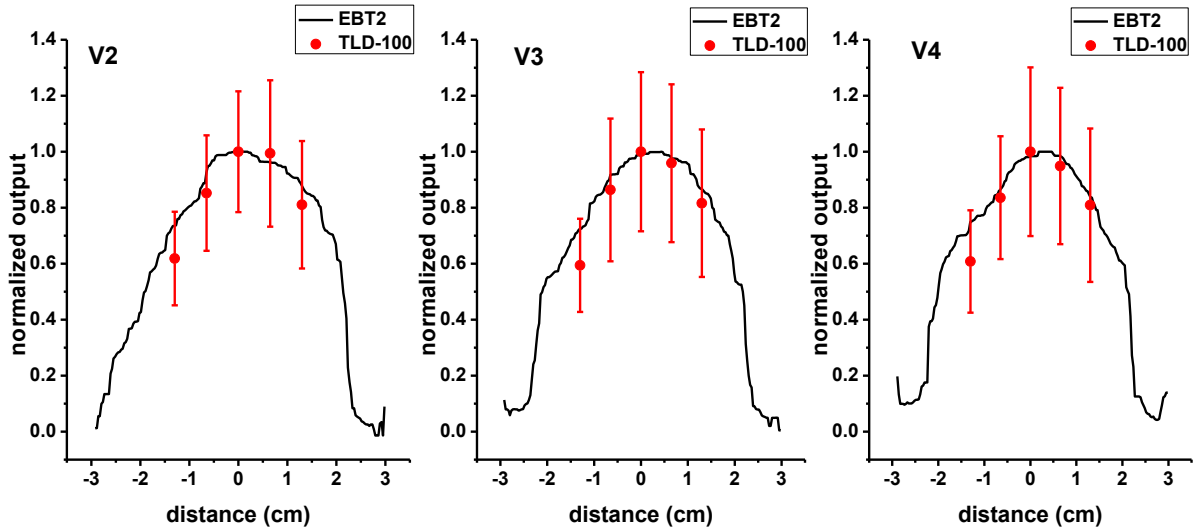

Figure 43: Horizontal profiles from EBT2 radiochromic film measurements. The profiles measured with TLD-100 are also show for comparison.

Different x-ray spatial distribution shapes have been measured in several devices. In [10], Knoblauch et. al measured hard x-ray distribution of PF 4.7kJ outside the discharge chamber by using TLD 700 when deuterium-argon mixture is used as working gas. This was anisotropic and presented a peak on the electrode axis. TLDs 200 were used to measure the x-ray distribution in a PF of 4.8 kJ when deuterium gas is used [82]. This distribution showed two maxima around the electrode axis. In [25] Pavez et. al also measured angular x-ray distribution by means of TLD 100 and a sharp cone of emission is observed. It is also mentioned that the x-ray distribution would depend on the anode geometry, in which the energetic electrons will collide, modifying the expected angular distribution for a Bremsstrahlung process.

4.2.5 Virtual source study

The x-ray emission output is measured by the IC and a TLD100 array when these detectors are placed at different distances from the plastic window of the PF2kJ device. The square root of the quotient between the intensity at the reference distance L_0 (chosen at 16.5 cm from the plastic window for both methods) and the intensity at a distance L is plotted for different distances in Figure 44 (a). It can be seen a linear trend. The last point from IC measurement is an outlier value in spite of the output corrections performed. The charge collected by the IC was in the order of 10^{11} C at the farthest distance from the source (~ 50 cm), that is one order higher that the background value (~10^{12} C). Then, the reason would not be that IC was not able

to measure there but possibly the IC measurement is not corrected properly by the PMT when the IC is placed closer to PMT (IC could eclipse PMT).

A linear regression is performed in order to estimate the position of the virtual source for each method separately and when it is considered both (Figure 44 (b)). The outlying measurement that was mentioned before is removed for fitting. The values that were obtained are shown in Table 6.

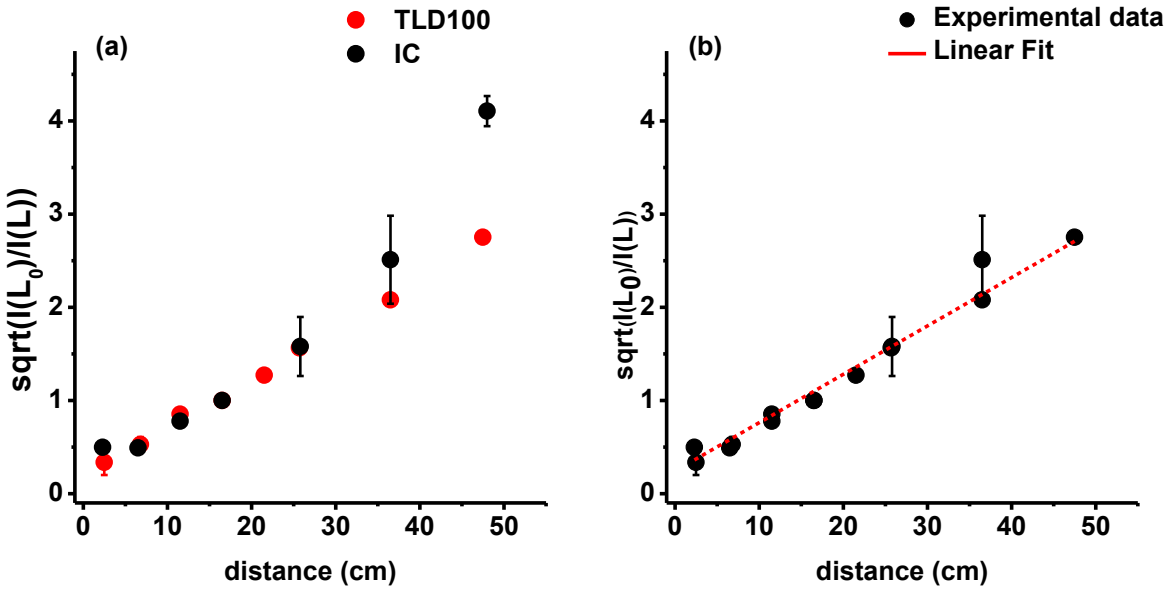

Figure 44: X-ray emission of PF2kJ depending on the distance. **(a)**The emission is measured by using IC (black) and TLD100 array (red). The readouts of these detectors are corrected by the output measured by PMT and TLD100 respectively. Error bars correspond to standard deviations, **(b)** Linear fit in order to estimate the position of the virtual source. The values from both measuring methods are considered for fitting.

Table 6: Estimation of the virtual source position of the x-ray source of the PF2kJ device by using two different detectors.

Method	Fit R-square	Virtual source position (cm)
TLD100	0.99	2.2 ±0.5
IC	0.67	11.5 ±1.4
Both	0.98	4.6 ±0.3

Different virtual source positions are obtained from the two different methods. Since IC measurements have the highest measurement errors, the R-squared value is the worst. But, when all data is used for the fitting procedure, the linear fit yields an R-squared value of 0.98 and an intercept with the abscissa axis representing the virtual source position of 4.6±0.9 cm below the plastic window and the error of the estimation of this value is the lowest compared with the other methods.

The position estimated in this study would be consistent since it locates inside the PF chamber, between the position of the plastic window and the anode base (at 15 cm). Then, the main emission of the PF2kJ device comes from 4.6 cm below the plastic window.

It is mentioned in [83] that the x-ray emission energy spectrum extending to tens of keV has its origin in Bremsstrahlung radiation from the acceleration of electrons through the ion field inside the plasma. X-ray emission of higher energies, is produced by the acceleration and collision of beams of electrons at the tip of the anode (energies above 100 keV) or by the emission of characteristic x-rays from elements with high atomic numbers that it can be observed in plasma column for neon and argon gases and in the anode region. Based on this, the next effective energy study (see 3.2.2.6) and the characteristics of the PF2kJ, the origin of the emission of this device should come from the plasma column. If it is considered that the column length ranges widely between the PF devices [84], [85] and the x-ray emission can occur along anywhere along the plasma column, the estimation of the position of the virtual source is consistent with the data reported in literature.

4.2.6 Effective energy

Figure 45 shows the transmission values (I/I_0) when different aluminium thicknesses are placed in front of the window of the device. It can be noticed that the plot is not linear for the two methods, therefore, the x-ray emission generated by PF2kJ is not monoenergetic. The error bars correspond to standard deviations and are the order of 20%.

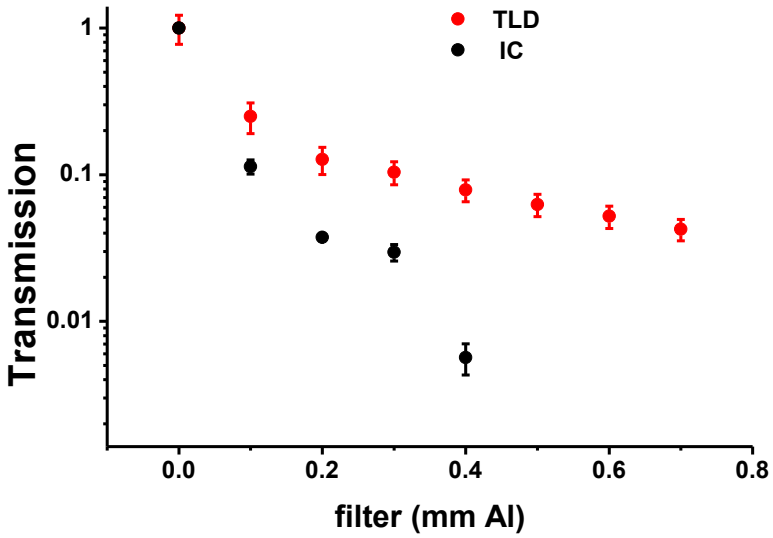

Figure 45: Transmission values for different aluminium thicknesses represented in logarithm scale when (a) TLD100 are used and (b) IC is used.

In spite of the different slopes for the two HVL measuring methods, it can be said that the HVL value is lower than 0.1 mm approximately for both methods, being the x-ray emission of low penetrability and the QVL value (transmission value of 0.25) is also lower than 0.1 mm. The effective linear attenuation coefficient is the same for HVL and QLV due to both values are between the first two points and therefore, the slope (attenuation coefficient) is the same. Thus, the homogeneity coefficient (HC) will be 0.5 by using the expression for exponential attenuation (see equation (5)). This HC value is consistent with the fact that the emission is not monoenergetic. To estimate the linear attenuation coefficient value, the slope of the curve is determined by performing a linear regression considering the first two points and the first three points of the curve. The HVL value is given by using the expression for exponential attenuation and the mass linear attenuation coefficient by dividing the linear attenuation coefficient by the density of the Aluminium (2.7 gr/cm^3). The linear attenuation coefficient and HVL values are shown in Table 7 for every experiment. The corresponding effective energy values are also shown, where the effective energy is estimated by interpolating between the two mass linear attenuation coefficient values nearest to the value determined, based on data from [72].

The thickness required to attenuate the beam to one tenth of its original intensity (TVL) is also calculated. Values of 0.02±0.002 mm and 0.01±0.002 mm are obtained by the two methods. This value is used in radiation protection to determine the

number of thicknesses required for shielding. It can be seen that in the case of PF2kJ shielding, a very thin thickness is required.

Table 7: Linear attenuation coefficient, HVL and effective energy values determined by measuring the transmission through different Aluminium thicknesses placed in front of the x-ray source of PF2kJ. The measurements are performed by using TLD100 and IC and output corrections are applied. The first two and three points of the curve in **Error! Reference source not found.** are considered in order to determine the above mentioned values.

Method	μ (1/cm)		HVL (mm Al)		E_{eff} (keV)	
	2 points	*3 points*	*2 points*	*3 points*	*2 points*	*3 points*
TLD100	138±42	109±10	0.05±0.01	0.06±0.01	8.0±0.5	8.8±0.3
IC	221±44	164±24	0.03±0.01	0.04±0.003	7.0±0.5	7.7±0.03

A low effective energy is obtained from the different experiments. When three points are used, the effective energy was a 10% higher. From the two measurements, a mean effective energy of 7.5 ± 0.5 is determined by averaging the results from the two methods. The effective energy value was higher when TLDs were used with respect to the value obtained with IC. The differences can be attributed to the fact that the measurements for the two methods were performed on different days and the x-ray spectrum may be different, in spite of the number of shots used in every measurement was the same and output corrections were applied.

Diagnostic energy of radiographic/CT x-rays are in the range 40–150 keV and for mammography beams, the photon energy is between 18 and 23 keV [86]. Then, the effective energy of the x-ray emission by the PF2kJ device is of lower energy than the diagnostic machines used in clinical routine.

This low effective energy value would be explained as will be described below. X-rays from the PF device depend upon many factors such as the applied voltage, operating pressure, gas composition, electrode parameters, insulator, material and length of the anode. Then, the characterization of the emission should be performed for each particular device. In spite of differences, a roughly estimated common spectrum of PF X-rays is proposed in [87] for PFDs with a copper anode. It consists mainly of characteristic K-shell radiation line of the copper superimposed to a

continuous low intensity Bremsstrahlung emission, whose photon energy extends up to several keV. Soft x-rays come from thermal mechanisms (thermal Bremsstrahlung emission in the hot plasma column). This spectrum is depicted in Figure 46 (a).

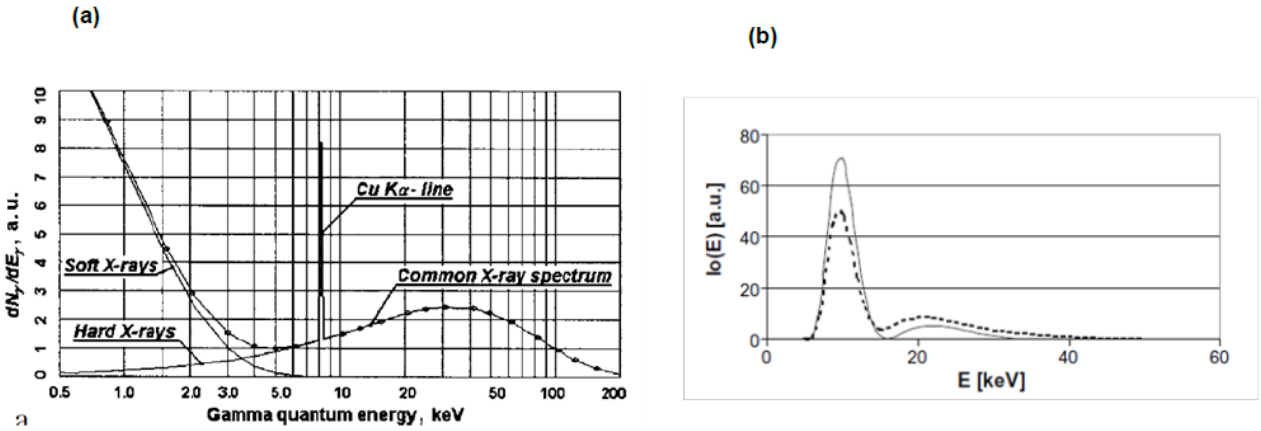

Figure 46: (a) A roughly estimated common spectrum of DPF X-ray (from **[87]**), **(b)** Calculated energy spectra of the X-ray measured in the axial window (…..) and in the lateral window of the device, taken from **[88]**.

The shape of this spectrum was observed in [87] for a PF of 175kJ- 406kJ with Hydrogen as working gas by means of multi-channel thermoluminescence dosimetry. The soft x-rays are filtered by the device (entrance window and others) such that only the peak of characteristic radiation and the tail are visible. Tartari et. al [88] calculated the energy spectra by a mathematical formalism and TLD 100 measurements by using the same method mentioned above, and they observed the same shape of the spectrum for a PF of 7kJ of copper anode and Hydrogen as filling gas. The shape presented a prominent peak near 10 keV followed by a tail of much lower intensity (Figure 46 (b)). Raspa et. al [8] also calculated the energy spectra of a PF of 5.7kJ of stored energy and copper anode when deuterium is used as working gas. The transmission values are measured by means of radiographic film and a single maximum around 60−80 keV is obtained followed by a tail of lower intensity. It can be see that for the devices mentioned before, the energy of the emission are the order of keV. A maximum is also present at lower energies that is consistent with the effective energy value estimated in this study.

A different effective energy was observed in [12] depending on the number of shots with effective presence of x-rays detected by a photomultiplier. In that study, Zambra et al. measured the transmission through different materials, as Pb, Cd, Ag, among

others, by using radiographic films. They used two different anode materials (Ag and Pb), and in both cases they noticed that the effective energy increases as the number of shots increases (see Figure 47), ranging from 32 to 102 keV. Since it is not mentioned if output variations occur in their device or whether output corrections are applied, these variations might be due to the output corrections (if not considered). In order to determine the effective energy dependence on the number of discharges, additional measurements should be performed in our device.

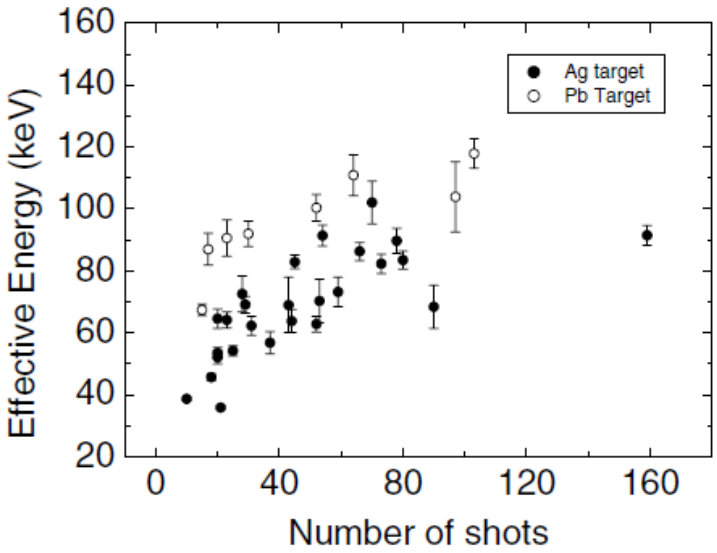

Figure 47: The effective energy against the number of shots for two different anode materials. The transmission through different materials is performed by using radiographic films. Taken from [12].

4.2.7 Radiation Protection

TLD 100 monitoring dosimeters were placed around the device during 70 days approximately in order to estimate the risk to operator personal exposed. During this time, a total of 2260 discharges were performed at different pressures. Most of the discharges (80%) were performed at 7 mbar (the pressure at which the highest x-ray emission is expected). The mean charge collected by TLDs 100 at each position for 2260 discharges are shown in Table 8. The mean value of the TLDs 100 charge collected was 2.62±0.88 nC.

Table 8: The mean charge collected in a period of 70 days by TLDs100. The mean charge from two TLD100 placed at each position is shown.

Mean charge (nC)			
Position 1	***Position 2***	***Position 3***	***Position 4***
2.02 ± 0.46	2.10 ± 0.07	2.45 ± 0.24	3.92 ± 1.03

Then, the conversion of the mean charge into $H_p(10)$ values was calculated by multiplying this value by the corresponding calibration factor is 0.43 ± 0.15 mSv. This is the personal equivalent dose value if the personal is approximately at 45 cm from the central axis of the device chamber and during a period of 70 days, under normal frequency of device use.

If the shots considered are those that emitted x-rays, based on the signal of the PMT, i.e., approximately 1800 discharges, the personal equivalent dose per shot is around 0.24 μSv. Based on this last value, it can be estimated the $H_p(10)$ value considering the worst case: the PF2kJ device is operated five days a week, the maximum number of shots allowed per day is performed (400 discharges), and the same operator operates the device every day being at 45 centimetres from the chamber of the device. In this case, he/she would receive 23 mSv per year. This personal dose equivalent value is almost below the dose constraints recommended by ICRP (20 mSv/year). But again, it is not a realistic case, but a worst scenario. In a more real scenario in which the operator is usually at least 100 centimetres from the chamber of the device in operating regime and the device is operated three days a week in average, the $H_p(10)$ value would be 2.8 mSv per year. This value is in the order of the values obtained by the dosimeters handled by the dosimetry department of CCHEN and used by the research personal (1.83-2.11 mSv/year).

It is important to mention that the $H_p(10)$ value here calculated an underestimation since the effective energy of the IC used for the x-ray TLD's cross calibration is around 15 keV and the effective energy of x-ray emission of the device is estimated at 8 keV. An extrapolation can be roughly performed from the data available in [60] in order to estimate the underestimation. A 45% is estimated and then, a $H_p(10)$ value of 4.1 mSv/year is obtained (realistic case), still within the recommended limits. In a worst scenario (device being used at maximum capacity), this value would be 33 mSv/year, being unsafe for research personal.

Based on the previous estimations and ICRP recommendations, this device should not present a high radiation risk for the operator. It is recommended to be careful if the equipment is used more frequently and the personnel are closer to it, because the device could be out of the accepted limits (23 mSv/year).

4.3 Neutron emission

The results of measurements performed to measure neutron emission from PF2kJ by using ^{3}He and pairs of TLD600 and 700 in different experimental setups are presented here.

4.3.1 Pressure efficiency for neutron emission

The pressure that maximizes the neutron emission is determined based on the ^{3}He detector. The normalized neutron emission depending on the filling pressure is shown individually for each series of measurements (see Figure 48). It is observed that the discharges previously performed act as warming for the next discharges, since in the first set of measurements the pressure decrease when the discharges are performed, in contrast to the second measurement stage, where the pressure increases with the discharges. In the first case (pressure lowering) it is noticed that the maximum emission is reached at 4 mbar and very low neutron emission is seen at higher pressures. In the other case (pressure increase), high neutron emission is observed at higher pressures (7 and 8 mbar), since more previous discharges are performed in comparison to the first case, being the emission slightly higher at 7 mbar than the emission at 4mbar (3% higher). However, the highest neutron emission is observed at 4mbar on average and this as working pressure value is chosen

Although the main objective of this pressure study is to set the ideal pressure, it is as well observed that the warming of the device may be important for the intensity of the neutron emission and this last one may be not reproducible shot to shot. Further studies should be performed regarding this issue.

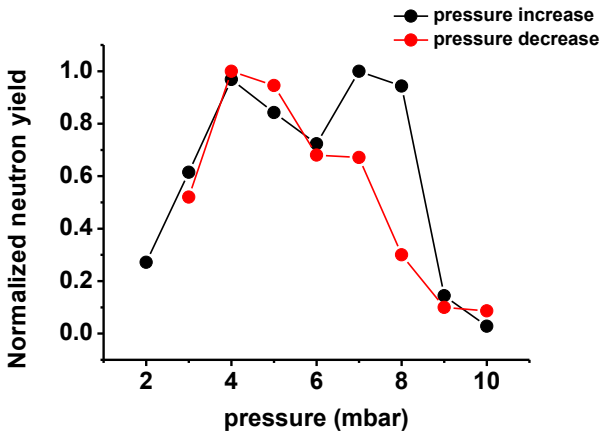

Figure 48: Neutron emission measurements against the filling gas pressure. It is shown as individual series: one serie is performed by increasing the pressure (black) and the other series is performed by decreasing the pressure (red).

4.3.2 Neutron emission measurements

4.3.2.1 TLD600-700 response varying the number of discharges

150 and 300 discharges with effective presence of neutron emission based on the He^3 signal are performed in order to determine the minimum number of shots necessary to see a distinct signal of neutron emission in the thermoluminescent dosimeters TLD 600. Three pairs of TLD 600 and TLD 700 are placed at 7 cm from the plastic window of the chamber with a polyethylene moderator of 5 cm. Table 9 shows the total neutron emission in a solid angle of 4π at 130 cm from the PF device for the two different numbers of discharges. Based on this yield value given by ^{3}He detector system, the number of neutrons per cm^2 can be estimated. It is also possible to estimate the neutron fluence in the axis direction (0° position) at 7 cm from the plastic window (which is the position in which the dosimeters were placed), assuming that neutron emission follows the inverse of the squared distance and applying the anisotropy factors found in literature (1.25 and 1.5). The values of neutron fluence estimated at 130 and 7 cm are shown in Table 9 too.

Table 9: Fast neutron yield in 4π at 130 cm of the side of the chamber (90°) when 150 and 300 discharges with effective neutron emission are delivered. Then, the fluence (n/cm^2) is estimated at 7 cms in the axis direction (0°). The anisotropy factors of 1.25 and 1.5 are applied.

Number of discharges	Position of the detector		
	(130 cm, 90°)		(7 cm, 0°)
	$Y_{4\pi}$	$\emptyset_n$ (n/cm^2)	$\emptyset_n$ (n/cm^2)
150	9.71x10^8	4.57x10^3	1.97x10^6 - 2.36x10^6
300	1.5x10^9	7.11x10^3	3.06x10^6 - 3.68x10^6

In spite of a fluence of fast neutron of ~10^6 n/cm^2 estimated by ^{3}He detector system at the positon where dosimeters are placed, the output from pairs of TLD 600-700 detector shows that the TLD system is not able to detect them in spite of 4 cm of moderator thickness used. No difference was found between TLD 600 and TLD 700 outputs when 150 discharges and 300 discharges are performed. The average difference between the pairs is 3 nC. Then only x-ray emission is detected for the two types of dosimeters corresponding to 0.8 ± 0.4 mSv and 0.6 ± 0.2 mSv for 150 and 300 discharges respectively at 7 cm of the plastic window, in terms of $H_p(10)$. The most of the glow curves (GCs) for the pairs of TLD 600-700 are similar as shown in Figure 49 (a). Figure 49 (b) shows GCs of dosimeters pair when the measurements are performed in a ^{241}Am-Be fast neutron source and it can be observed a difference between the two types of dosimeters, in contrast to Figure 49 (a).

It can be observed that when the number of shots was the double, the fast neutron emission increased 1.6 times

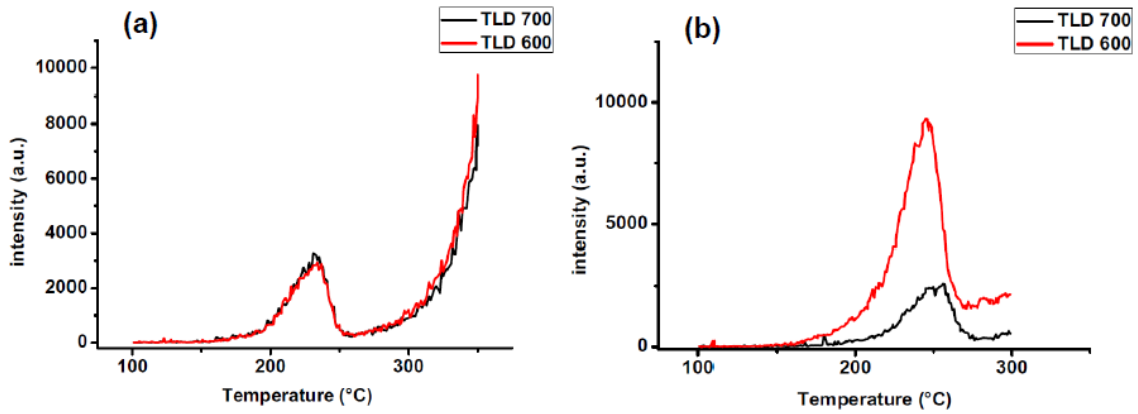

Figure 49: **(a)** An example of glow curves of TLD 600 and TLD 700 detectors from the measurements carried out in presence of mixed neutron photon emissions generated by PF2kJ device. The glow curves corresponds to 150 discharges performed in D_2 gas. **(b)** An example of glow curves of TLD 600 and TLD 700 detectors from the measurements in a ^{241}Am-Be fast neutron source.

4.3.2.2 TLD600 and TLD700 responses varying the moderator thickness

450 discharges were performed in D_2 gas with effective presence of neutron emission when three TLD arrays composed of three pairs of TLD 600 and TLD 700 are used to detect the emission. These three arrays are placed at 2, 5 and 7 cm from the plastic window. Polyethylene slabs of 4 and 5 cm are placed before the arrays that are placed at 5 and 7 cm, respectively. The first TLD array is placed without moderator. The different thicknesses of material for thermalizing the neutrons are used in order to find the thickness that enhances the response of the TLD 600, since the cross section of TLD 600 is almost 10^4 times higher for thermal neutrons compared with TLD 700. 160 of the 450 total shots (corresponding to 35% of the total shots) are delivered at the pressure at which the highest neutron emission is observed (4 mbar). However, the response of the TLD 600 and TLD 700 is the same in the different setups for moderating, as it can be observed in the glow curves shown in Figure 50. The red and black lines correspond to TLD600 and 700 glow curves respectively when any material for moderating is used (Figure 50(a)), when 4 cm of polyethylene is used (Figure 50(b)) and when 5 cm of polyethylene material is placed before the TLD array (Figure 50(c)).

Then, the pairs of TLD 600 and 700 only detected x-ray emission. The size of the glow curves decrease when more moderator thickness is added since the x-rays are more attenuated. Based on this, it can be estimated the HVL and effective energy considering that the polyethylene moderator is a filter of 0.93 gr/cm3 density. The transmission values and the values of HVL, linear attenuation coefficient and effective energy estimations are shown in Table 10. The HVL value is given by the interpolation between the two first points and the linear attenuation coefficient from the slope.

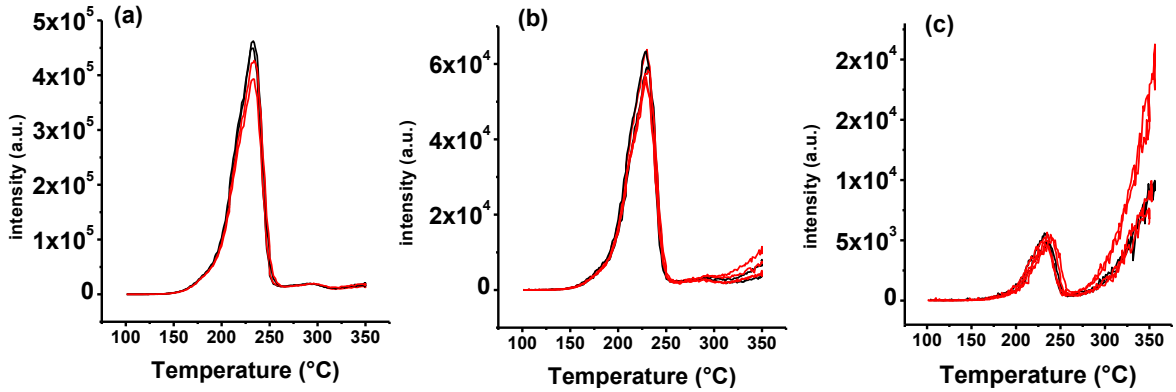

Figure 50: Glow curves for TLD600 (black) and TLD 700 (red) when **(a)** no moderator is used, **(b)** a thickness of 4cm polyethylene is used and **(c)** 5 cms of polyethylene is used for thermalizing. 450 discharges were delivered for all configurations.

Table 10: Transmission values, HVL, linear attenuation coefficient and effective energy estimations from TLD 600-700 measurements when 4 and 5 cm of polyethylene act as filter.

Polyethylene (cm)	Transmission	Estimation
		HVL (cm)
0	1 ±0.11	2.3 ± 0.5
		Linear attenuation coeff. (cm^{-1})
4	0.14 ±0.02	0.5 ±0.05
		Effective energy
5	0.03 ± 0.01	18 keV

The effective energy value is higher compared to the energy when it is only photon emission (see section 4.2.6). The reason may be as explained below. As an example, estimations of attenuations by using an online tool (X-ray attenuation & absorption calculator) [89] are 9% and 80 % when filters of 0.1 mm Al and 40 mm polyethylene (they are the first filters used in the cases of only photon emission and mixed emission respectively) are considered for a monoenergetic emission of 20 keV. Based on these estimations and considering a polyenergetic emission this time, the lower energies may be less attenuated in the first case compared to the second and then, the effective energy value should be lower. The number of discharges delivered in the two studies was also different and the average energy of the emission would become more evident while the number of discharges increases considering the low reproducibility shot to shot of the emission. In spite of this difference, the effective energy value is in the order of tens of keV (as it had been determined in section 4.2.6).

On the other hand, the ^{3}He detector system detected fast neutron emission. The results of the total neutron yield in a solid angle of 4π sr at 130cm from the PF device and the estimation of the fluence of fast neutrons based on these neutron yield values are shown in Table 11 at the distances of 130 cm (^{3}He detector position), 2, 6 and 7 cm.

Table 11: Fast neutron yield in 4π at 130 cm of the side of the chamber (90°) when 450 discharges with effective neutron emission are delivered. Then, the fluence (n/cm^2) is estimated for positions at 2, 6, and 5 cms in the axis direction (0°). The anisotropy factors of 1.25 and 1.5 are applied.

Number of discharges	Position of the detector				
	(130 cm, 90°)		(2 cm, 0°)	(6 cm, 0°)	(7 cm, 0°)
	$Y_{4\pi}$ (N° of neutrons)	$\emptyset_n$ (n/cm^2)	$\emptyset_n$ (n/cm^2)	$\emptyset_n$ (n/cm^2)	$\emptyset_n$ (n/cm^2)
450	2.08x10^9	9.78x10^3	5.16x10^7-6.20 x10^7	5.74x10^6-6.88 x10^6	4.22x10^6-5.06x10^6

Since it was not feasible to obtain a clear difference between the responses of TLD 600 and 700 for any of the configurations or by increasing the number of shots, it is not possible to measure neutron emission generated by the PF2kJ device by using pairs of TLD 600 and 700, while in the helium detector it was possible to obtain signals that indicate the presence of fast neutrons.

From the Table 9 and Table 11, the total fast neutron yield per shot can be calculated. Yields of $5x10^6$, $6.5x10^6$ and $5x10^6$ neutrons are obtained by dividing the $Y_{4\pi}$ by the number of total discharges. These values are in agreement with empirical scale law for total neutron production per discharge when D-D reactions occur. This law is $(Y_n)_{D\text{-}D} \approx \Lambda\ E_c^2$ (n/shot), where Λ is between 10^6 and 10^7 if E_c is given in kJ [34]. In this case, the E_C value corresponds to 2.

It is needed to estimate the thermal neutron fluence for explaining the no signal of neutron presence in TLD 600. In order to do it, a MC simulation was made by Dr. Francisco Molina and Byron Parra, who belong to Nuclear Applications Department from CCHEN. A starting number of 10^6 fast neutrons of 2.3 MeV through 4 and 8 cm of polyethylene in an area of 20 x 20 cm^2 were simulated. Transmission values of 30% and 16% were estimated for the different thicknesses respectively. The energy of the transmitted neutrons ranged between 10^{-9} MeV and 1 MeV as shown in Figure 51. Based on this simulation, a neutron fluence around 10^4 n/cm^2 with 4 and 5 cm moderator thicknesses can be estimated for the actual case, considering only neutrons with energies between 10^{-9} MeV and 10^{-2} MeV, energy interval where the neutron response difference between TLD 600 and TLD 700 are considerable (3 to 4 order of difference) [90]. While it has been reported that these dosimeters can be used for fluence measurements in low thermal neutron fluences from 10^4 to 10^{12} [91], it was not possible to measure them in this device since this fluence value is at the lowest sensitivity limit of TLD detection. However it has been possible to measure neutron emission by using this pair of dosimeters in other PF devices but higher yield per shot has been reported, as it can be noticed below.

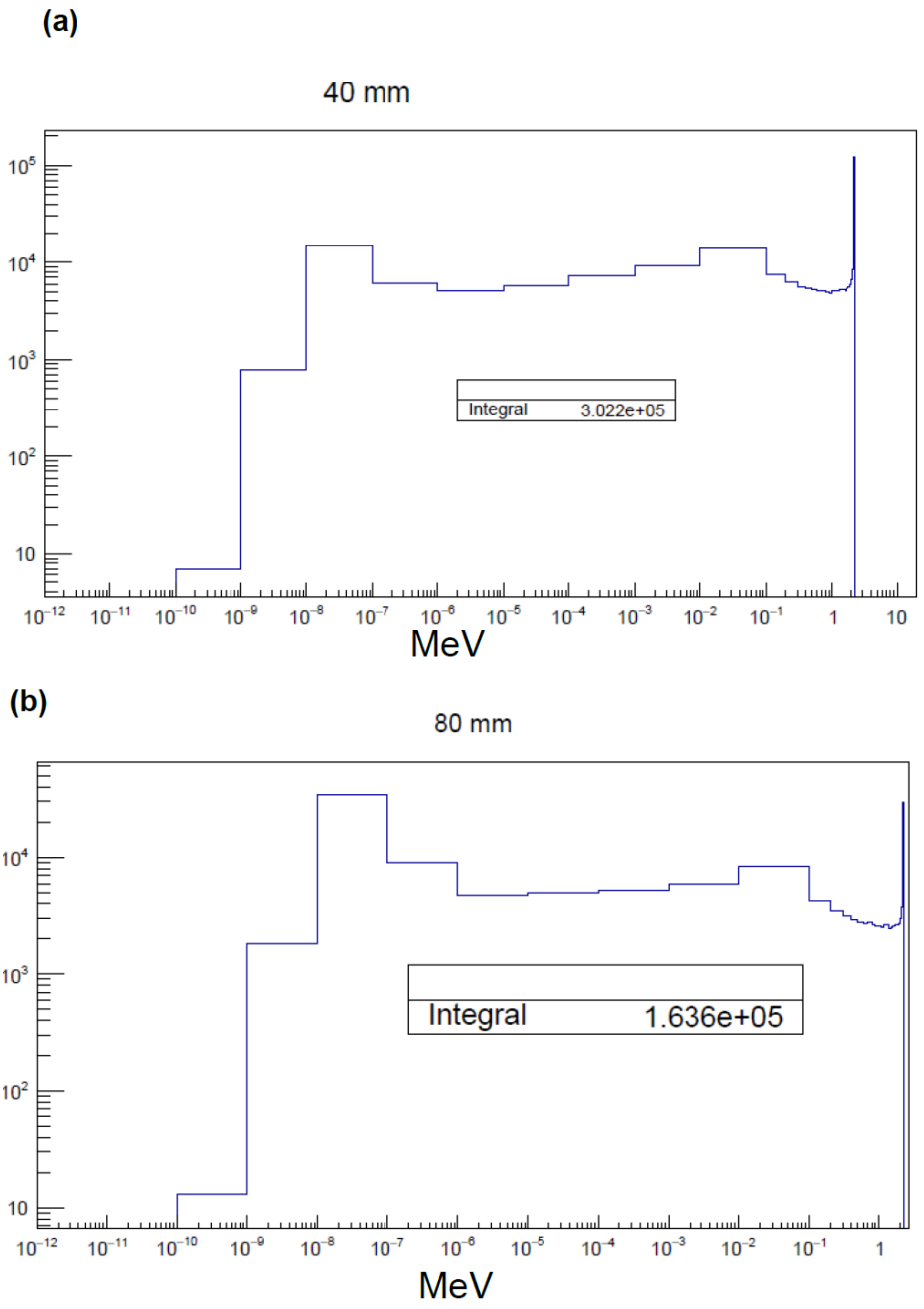

Figure 51: MonteCarlo simulation for an initial fluence of fast neutrons of 2.3 MeV through **(a)** 40 mm and **(b)** 50 mm of polyethylene moderator thicknesses.

The highest fast neutron fluence estimated in our neutron measurements is the order of ~10^7 n/cm^2 at 2 cm from the plastic window when 450 shots are delivered. The fast neutron fluence can be roughly estimated at 2 cm of the plastic window giving a value of the order of ~10^5 n/cm^2 per shot when the discharges are performed at 4mbar. In a PF-1000 device of 1MJ of stored energy [92], the average fast neutron yield per discharge was obtained from the silver activation detectors, being the order of 10^{11}n/shot. This information was useful in order to determine the shots required to

obtain optimal readings of pairs of TLD 600 and 700 placed at Bonner spheres in order to determine the spectra of neutrons. In a PF device of 4.8kJ of stored energy [93], an average yield of (5.3±0.5)x10^8 fast neutrons per shot into 4π sr was obtained. The yield for each shot was measured by two calibrated Geiger-Muller activation counters. As safety purpose, dosimetric measurements were carried out by using TLD 600 and TLD 700 dosimeters placed at different distances from the source when several discharges were performed. It can be notice that the yield per shot obtained in these PF devices is much higher than the yields obtained in this work for high number of discharges such an important number of discharges would be needed (being impractical for this device).

Despite it was not possible to measure the neutron emission by using pairs of TLD 600 and TLD 700, the studies performed in this work could be a preliminary research since the main of the discharges were not performed at the ideal pressure at which the neutron emission is the highest. It is estimated that a total of 1000 discharges at this pressure are required to reach a fast neutron emission of 10^8 n/cm^2. In the research mentioned in [93], equivalent neutron doses of 0.019 mSv/shot are estimated for this fluence at 2.54 m from the source, behind a 80 cm thick concrete brick wall.

5. Conclusion and outlook

The PF2kJ device is a pulsed radiation source of special interest due to its several applications. In this work, an extensive characterization of its x-ray emission and a monitoring of its neutron emission were performed.

In regard to the x-ray emission produced when the filling gas is Hydrogen, the pressure that maximizes the emission was determined. It was observed that the x-ray emission is different for different discharges. For that reason, an output correction factor is needed in order to correct the measurements performed to further analyze other parametric dependences. For this, two monitoring systems were used, TLDs and PMT signal.

A clear linear correlation (of 0.95) between the area under curve of the PMT signal and the output measured by TLD100 dosimeters was found 3.21×10^{7} ± 5% nC/Vs. This correlation would allow determining the dose output without the use of thermoluminescent dosimeters and only through the photomultiplier signal acting as a surrogate detector. This would require a proper cross calibration using the TLD 100 dosimeters (previously calibrated in absorbed dose or personal dose equivalent terms). In particular, since studies regarding irradiation of cancer cells in a pulsed source are being carried out in this device, this method would make easier the estimation of the dose [9] with an uncertainty lower than 10%.

By performing measurements with TLD 100 and radiochromic film, the distribution of the x-ray emission is observed to be non symmetrical in both axis (up to 6% of asymmetry). For both methods the biggest difference was between the intensity at the central axis of the device and the intensity at 2 cm from the axis in the lower region, corresponding to 43%. A FWHM value of 4 cm approximately is estimated. Different x-ray distributions of PFDs are found in literature, where the angle around the symmetry axis is principally determined by the geometric characteristics of the anode cavity in the upper region of the anode.

It was observed that the intensity of the x-ray emission varies inversely with the squared of the distance for this particular pulsed source. Then, the virtual source could be determined to be at 5±7% cm below the plastic window of the device. Since several processes inside the dense column plasma produce the x-ray emission, the position that was determined is in agreement with the plasma dynamics.

An effective energy of 7.5±0.5 keV could be estimated by using TLD 100 and IC detectors, that corresponds to HVL of 0.06±0.01 mm. This value is lower compared with diagnostic devices used in clinical routine. The effective energy of the order of keV is consistent with the spectrum proposed and also measured in some works for a PF device with copper anode. The determination of the energy of the x-ray emission may be important when TLD dosimeters are used to evaluate dose values since they have a response that depends on the photon energy as well as to know the penetrability of the emission with a view to radiation protection. Transmission measurements should be performed by using other filter materials to support the

results obtained in this study and in order to estimate the spectrum by means of the technique described in [8]; as well as studies where the number of shots varies, since it seems that the effective energy value may depend on it, based on the conclusions in [12]. As a proposal measurement, several material thicknesses should be used at the same time by arranging them as stairs and place dosimeters before and after of each thickness in order to remove output dependence.

It is essential to assess the exposure levels of x-ray emission at which the device operators may be exposed. In this work, the personal dose equivalent obtained is 2.8 mSv/year, within the dose constraints recommended by the ICRP (20mSv/year, averaged over 5 years and not exceed 50 mSv in any single year). This value is in the order of $H_p(10)$ values measured by the dosimetry department of CCHEN. If energy dependence of the response of TLD 100 is taken into account, a value of 4.5 mSv/year is estimated. In the worst case scenario, where the device is operated at maximum capacity and the operator is very close to it (~40 cm), a $H_p(10)$ value of 23 mSv/year may be registered.

With regard to neutron emission produced when the filling gas is Deuterium, the pressure that maximizes the emission was determined with ^{3}He detector. A higher effective energy for x-ray emission is estimated by using TLD 600 and TLD 700 signals. Differences in effective values may be attributed to different number of discharges delivered and the different filters used.

The highest fast neutron fluence estimated by using ^{3}He detector was of the order of 10^5 n/cm^2 per shot and a thermal fluence of 10^4 n/cm^2 could be estimated by MC code when 4 and 8 cm of moderator was used. In spite of this fluence should be enough according to [91] for obtaining a signal in TLD 600 dosimeters that indicates the presence of thermal neutrons, this fluence value is at the lowest sensitivity limit of TLD detection. It was not possible to detect any signal above background and distinguishable from the x-ray emission despite having used different thicknesses of moderator to thermalize the neutrons and thus, more studies should be carried out. Measurements by using TLD 600-700 were successful in other PF devices reported in literature, when higher neutron fluence is emitted.

The energy of the neutron emission should be also determined in order to estimate the ideal thickness to thermalize the neutrons by means of TOF technique [14]. In this work it is assumed that the energy corresponds to 2.45 MeV based on the premise that the emission occurs by means of D-D fusion. However, low neutron energy variations have been measured from 1 MeV to 3.5 MeV [46], [77] in different deuterium filled PFDs. The number of discharges required for obtaining a minimum response in TLD 600 should be determined by totally attenuating the x-ray emission with the aim to perform the measurements by using only TLD 600. Then, dosimetry measurements when a mixed neutron-gamma radiation is present should be carried out in order to assess the personal exposition to this radiation by means of TLD 600 and TLD 700 measurements.

Bibliography

[1] T.I. Filipova, V.P. Vinogradov N.V. Filippov, "High-Temperature Dense Plasma in the Region of the Noncylindrical Z-Pinch," *Nucl. Fusion*, p. 577, 1962.

[2] J.W. Mather, "Formation of a high-density deuterium plasma focus," *Phys. Fluids*, vol. 8, no. 2, pp. 366-377, 1965.

[3] G.M. El-Aragi, "Low energy plasma focus simulate astrophysical phenomena," *JOPA*, vol. 4, no. 1, 2016.

[4] A. Bortolotti, "Inspection of extended objects with fast neutrons: numerical tests," *Nucl. Instrum. Method B*, vol. 63, no. 4, 1992.

[5] A. Tartari, "Improvement of calibration assessment for gold fast-neutron activation analysis using plasma focus devices," *Meas. Sci. Technol.*, vol. 13, no. 6, 2002.

[6] S. Hussain, "Plasma focus as a possible x-ray source for radiography," *Plasma Sources Sci. Technol.*, vol. 14, no. 1, 2005.

[7] A. Tartari, "Feasibility of X-ray interstitial radiosurgery based on plasma focus device," *Nucl. Instrum. Method B*, vol. 213, 2004.

[8] C. Moreno, L. Sigaut and A. Clausse V. Raspa, "Hard x-ray spectrum emitted by a plasma focus optimized for flash radiography," *Phys. Scr.*, vol. 2008, no. T131, 2008.

[9] J. Jain et al., "Hundred joules plasma focus device as a potential pulsed source for in vitro cancer cell irradiation," *AIP advances*, vol. 7, no. 8, 2017.

[10] P. Knoblauch, "Hard X-ray dosimetry of a plasma focus suitable for industrial radiography," *Radiation Physics and Chemistry*, vol. 145, 2018.

[11] V. Dubrovsky, "On the Possible Mechanisms of Activation Changes of Enzymes under Pulsed Irradiation," *Journal of Russian Laser Research*, vol. 24, no. 4, 2003.

[12] M. Zambra, "Experimental results on hard x-ray energy emitted by a low-energy plasma focus device: a radiographic image analysis," *Plasma Physics Controlled Fusion*, vol. 51, no. 12, 2009.

[13] L. Soto, "Research on pinch plasma focus devices of hundred of kilojoules to tens of joules ," *Braz. J. Phys.*, vol. 34, no. 4b, 2004.

[14] J. Moreno , "Neutron energy distribution and temporal correlations with hard x-ray emission from a hundreds of joules plasma focus device," *Plasma Phys. Control. Fusion*, vol. 57, no. 3, 2015.

[15] A. Fabbri, "Radiation protection of PFMA-1, a plasma focus for medical applications," *J. Radiol. Prot.*, vol. 27, pp. 465–470, 2007.

[16] R. Amrollahi and M. Habibi M. J. Nemati, "Analysis for Radiation and Shielding Dose in Plasma Focus Neutron Source using FLUKA," *J Fusion Energ.*, vol. 31, 2012.

[17] F. Paschen, *Wied.Ann.*, vol. 37, pp. 69-96, 1889.

[18] J.N. Feugeas, "The influence of the insulator surface in the plasma focus behavior," *J.App.Phys.*, vol. 66, pp. 3467-3471, 1989.

[19] Rajdeep Singh Rawat, Ed., *Plasma Science and Technology for Emerging Economies: An AAAPT Experience*.: Springer, 2017.

[20] A. Bernard et, "Scientific status of plasma focus research," *J. Moscow Phys. Soc.*, vol. 8, pp. 106-108, 1998.

[21] S. Lee and A. Serban, "Dimensions and lifetime of the Plasma Focus Pinch," *IEEE TRANSACTIONS ON PLASMA SCIENCE*, vol. 24, no. 3, pp. 1101-1104, June 1996.

[22] J.W. Mather, "Formation of a high-density deuterium plasma focus," *Phys. Fluids*, vol. 8, pp. 366-377, 1965.

[23] H. Bruzzone, "The role of anomalous resistivities in Plasma Focus discharges," *Nucleonika*, vol. 46, no. 1, 2001.

[24] D.H. Sharp, "An overview of Rayleigh-Taylor Instability," *Physica D*, vol. 12, no. 1-3, 1984.

[25] C. Pavez, "Potentiality of a small and fast dense plasma focus as hard x-ray source for radiographic applications," *Plasma Phys. Control. Fusion*, no. 54, 2012.

[26] H. Acuña, and A. Clausse H. Bruzzone, "Neutron Correlations with Electrical Measurements in a Plasma Focus Device," *Brazilian Journal of Physics*, vol. 38, no. 1, March 2008.

[27] Jalaj Jain, *Studies on plasma focus devices and characterization of pulsed neutron and x-ray emission for cancer cell irradiation*. Chile, 2017, Thesis work, University of Talca.

[28] N. K. Neog, and T. K. Borthakur N. Talukdar, "Study on neutron emission from 2.2kJ plasma focus device," *PHYSICS OF PLASMAS*, no. 21, 2014.

[29] G. Pross, G.Decker and M. Trunk T. Oppenlander, "Plasma Phys.," no. 19, p. 1075, 1977.

[30] J.R. Smith, "Operation of a plasma focus device as a compact electron accelerator," *Phys. Fluids*, vol. 28, 1985.

[31] A. K. Dulatov, "Generation of hard X-ray emission by the electron beam in plasma focus facilities," *Plasma Phys. Rep.*, vol. 40, no. 11, pp. 902–909, November 2014.

[32] G. Gerdin, F. Venneri W.Stygar, "Particle beams generated by a 6–12.5 kJ dense plasma focus," *NUCLEAR FUSION*, vol. 22, no. 9, 1982.

[33] D. A. Meskan, and H. L. L. van Paassen M. J. Bernstein, "Space, Time, and Energy Distributions of Neutrons and X Rays from a Focused Plasma Discharge," *Phys. Fluid.*, vol. 12, no. 10, 1969.

[34] J.W. Mather, "Dense plasma focus," *Methods in Experimental Physics*, vol. 9, Part B, p. 225, 1971.

[35] A.K. Dulatov, "Generation of hard X-ray emission by the electron beam in plasma focus facilities," *Plasma Phys. Rep.*, vol. 4, no. 11, pp. 902-909, 2014.

[36] H Bruzzone, H Acuña, L Soto, A Clausse M Barbaglia, "Experimental study of the hard x-ray emissions in a plasma focus of hundreds of Joules," *Plasma Phys. Control. Fusion*, vol. 51, no. 4, 2009.

[37] P. Knoblauch, F. Di Lorenzo, C. Moreno V. Raspa, "Plasma focus based flash hard X-ray source in the 100 keV region with reproducible spectrum," *Phys. Lett. A*, vol. 374, no. 46, pp. 4675-4677, 2010.

[38] V. Raspa, L. Sigaut, R. Vieytes C. Moreno, "Plasma-focus-based tabletop hard x-ray source for 50 ns resolution introspective imaging of metallic objects through metallic walls," *Appl. Phys. Lett.*, vol. 89, 2006.

[39] E. Angeli , "Development of diagnostic tools for Plasma Focus derived X-ray source," *Nukleonika*, vol. 51, no. 1, pp. 15-20, 2006.

[40] V. Raspa, P. Knoblauch, A. Lazarte, C. Moreno, and A. Clausse F. Di Lorenzo, "Hard x-ray source for flash radiography based on a 2.5 kJ plasma focus," *Journal of Applied Physics*, vol. 102, no. 3, 2007.

[41] M. Bernstein, "Acceleration Mechanism for Neutron Production in Plasma Focus and z-pinch discharges," *Phys. Fluids*, vol. 13, no. 11, 1970.

[42] U. Jäger and H. Herold, "Fast ion kinetics and fusion reaction mechanism in the plasma focus," *Nuclear Fusion*, vol. 27, no. 3, 1987.

[43] S.P. Moo, C.K. Chakrabarty, and S. Lee, "An investigation of the ion beam of a plasma focus using a metal obstacle and deuterated target," *IEEE Transactions on Plasma Science* , vol. 19, no. 3, pp. 515 - 519, 1991.

[44] J.P. Rager, "The Plasma Focus," in *Unconventional approach to fusion*, B. Brunelli and G. G. Leatta, Ed.: Plenum Press, New York, 1982, p. 157.

[45] N. K. Neog, and T. K. Borthakura) N. Talukdar, "Study on neutron emission from 2.2 kJ plasma focus device ," *Physics of Plasmas*, vol. 21, no. 6, June 2014.

[46] L. Soto , "Demonstration of neutron production in a table-top pinch plasma focus device operating at only tens of joules," *J. Phys. D: Appl. Phys.*, vol. 41, no. 20, pp. 205-215, 2008.

[47] M.M. Milanese and J.O. Pouzo, "Evidence of non-thermal processes in a 1-MJ plasma focus device by analysing the neutron spectra," *Nuclear Fusion*, vol. 18, no. 4, p. 533, 1978.

[48] F.Mezzetti, F.Rocchi and M.Sumini V.Benzi, "Feasibility analysis of a Plasma Focus neutron source for BNCT treatment of transplanted human liver," *Nucl. Instrum. Method B*, vol. 213, 2004.

[49] F. Castillo-Mejía, "Small plasma focus studied as a source of hard X-ray," *IEEE Transactions on Plasma Science*, vol. 29, no. 6, 2001.

[50] S. Zapryanov, "Measurements of the Basic Characteristics of the Dense Plasma ," *Bulg. J. Phys.*, vol. 38, pp. 184–190, 2011.

[51] ISO, "Radiological protection characteristics of reference pulsed radiation," ISO, ISO/NP TS 18090, 2012.

[52] IEC, "Radiation protection instrumentation-Electronic counting dosimeters for pulsed fields of ionizing radiation," IEC, IEC/TS 62743, 2012.

[53] R. S. Rawat, "Dense Plasma Focus: Novel Tool for Plasma Nanotechnology," *Natural Sciences and Science Education*, National Institute of Education, Nanyang Technology.

[54] William R. Leo, "Scintillation Detectors," in *Techniques for Nuclear and Particle Physics Experiments: A How-to Approach*.: Springer, 1987, ch. 7, pp. 149-163.

[55] Claudio Furetta, *Handbook of Thermoluminescence*.: World Scientific Publishing Co. Pte. Ltd., 2003.

[56] Y.S. Horowitz, *Themoluminescence and thermoluminescent dosimetry*.: CRC Press, 1984, vol. 1.

[57] J. M. Gomez-Rosz and J. W.N. Tuynx G. Kitisy, "Thermoluminescence glow-curve deconvolution functions for first, second and general orders," *J. Phys. D: Appl. Phys*, vol. 31, pp. 2636–2641, 1998.

[58] S.W.S. McKeever, *Thermoluminescence of solids*.: Cambridge University Press.

[59] N. Suntharalingam, & G.N. Kenney J.R. Cameron, *Thermoluminescent dosimetry*. U.S.A: University of Wisconsin Press, 1968.

[60] S.D. Davis , J. A. Micka , L.A. DeWerd A.A. Nunn, "LiF:Mg,Ti TLD response as a function of photon energy for moderately filtered x-ray spectra in the range of 20-250 kVp relative to 60Co," *Med. Phys.*, vol. 35, no. 5, pp. 1859-69, 2008.

[61] P.S. Kim and P.S. Moon Y.S. Yoo, "A study on the neutron dosimetry with LiF thermoluminescent dosimeters," *Journal of the Korean Nuclear Society*, vol. 7, no. 3, 1975.

[62] "Technical Recommendations for the Use of Thermoluminescence for Dosimetry in Individual Monitoring for Photons and Electrons from External Sources," Commission of the European Communities, EUR , 5358, 1975.

[63] Glenn F. Knoll, *Radiaton detection and measurement*, 4th ed.: Wiley.

[64] P. Andreo, "Absorbed dose determination in external beam radiotherapy: An international code of practice for dosimetry based on standards of absorbed dose to water," IAEA, Viena, TRS 389, 2000.

[65] J. Sorenson, M. Phelps S. Cherry, *Physics in nuclear medicine*, 4th ed., Elsevier, Ed., 2012.

[66] T.W. Crane and M.P. Baker, "Neutron detectors," in *Passive non destructive assay of nuclear materials*, D. Reilly et al, Ed., 1991, ch. 13, p. 379.

[67] Indra J. Das, Ed., *Radiochromic Film: Role and Applications in Radiation Dosimetry*.: CRC Press, 2017.

[68] Reinhardt, "Comparison of Gafchromic EBT2 and EBT3 films," *Med. Phys.*, vol. 38, no. 8, August 2012.

[69] J.E. Villarreal-Barajas and R.F. Khan, "Energy response of EBT3 radiochromic films: implications for dosimetry in kilovoltage range," *J Appl Clin Med Phys.*, vol. 15, no. 1, 2014.

[70] M.J.Butson, "Energy response of the new EBT2 radiochromic film to x-ray radiation," *Radiation Measurements*, vol. 45, no. 7, pp. 836-839, 2010.

[71] McKetty MH., "Physics tutorial for residents. X-ray attenuation," *Radiographics*, vol. 18, no. 1, 1988.

[72] J. H. Hubbel and S.M. Seltzer. Tables of X-ray Mass attenuation coefficients and mass energy-absortion coefficients.

[73] Ministerio de Salud Chile. (1985, April) Dirección del Trabajo, Gobierno de Chile. [Online]. http://www.dt.gob.cl/legislacion/1624/articles-79239_recurso_1.pdf

[74] G.M. El-Aragi, "Scattered ionizing radiations from low energy focus plasma and radiation dosimetry assessment," in *Proceedings of the 7th Conference on Nuclear and Particle Physics,* Sharm El-Sheikh, Egypt, 2009.

[75] F.A. Stewart, "ICRP statement on tissue reactions and early and late effects of radiation in normal tissues and organs-threshold doses for tissue reactions in a radiation protection context," *Ann. ICRP*, vol. 42, no. 1, 2012.

[76] ICRP 2007, "The 2007 Recommendations of the International Commission on Radiological Protection," *Ann. ICRP 37*, p. 64, ICRP Publication 103.

[77] A. Tarifeño-Saldivia, "Calibration methodology for proportional counters applied to yield measurements of a neutron burst," *Rev. Sci. Instrum.*, vol. 85, 2014.

[78] J. Moreno, "System for measurement of low yield neutron pulses from D–D fusion reactions based upon a 3He proportional counter," *Meas. Sci. Technol.*, vol. 19, 2008.

[79] Sinha Roy Gambarini G., "Dependence of TLD Thermoluminescence Yield on Absorved Dose in a Thermal Neutron Field," *Appl. Radiat. Isot.*, vol. 48, pp. 10-12, 1997.

[80] F.N. Beg, "Study of x-ray emission from a table top plasma focus and its application as an x-ray," *J. Appl. Phys.*, vol. 88, no. 6, 2000.

[81] Castillo-Mejía, "Small Plasma Focus studied as a source of hard X-Ray," *IEEE TRANSACTIONS ON PLASMA SCIENCE*, vol. 29, no. 6, December 2001.

[82] et. al Castillo F., "Angular distribution of fusion products and x rays emitted by a small dense plasma focus machine," *JOURNAL OF APPLIED PHYSICS*, vol. 101, 2007.

[83] Babak Shirani Bidabadi Seyed Milad Miremad, "Measurement of the effective energy of pulsed x-rays emitted from a Mather-type plasma focus device," *Applied radiation and isotopes*, pp. 169-175, 2017.

[84] M. Liu, X. Feng, S.V. Springham, "Soft X-ray yield measurement in a small plasma focus operated in neon," *IEEE Trans. Plasma Sci.*, vol. 26, no. 135, 1998.

[85] A. Kasperczuk, R. Kumar, R. Miklaszewski, "tudy of the plasma evolution in the PF-1000 device by," *Physica Scripta*, vol. 65, no. 96, 2002.

[86] S. Christofides, A.D.A. Maidment, I.D. McLean, K.H. Ng D.R. Dance,.: IAEA, 2014, ch. 5 & 7, p. 174 & 215.

[87] V. Dubrovsky et. al, "Dense Plasma Focus as a powerful source of monochromatic X-ray radiation," *Nukleonika*, vol. 51, pp. 21-28, 2006.

[88] A. Tartari et. al, "Energy spectra measurements of X-ray emission from electron interaction in a dense plasma focus device," *Nuclear Instruments and Methods in Physics Research B*, vol. 213, pp. 206-209, 2004.

[89] G. Weber. X-Ray attenuation & absorption calculator. [Online]. https://web-docs.gsi.de/~stoe_exp/web_programs/x_ray_absorption/index.php

[90] Hsu F. Y. et. al, "Estimation of photon and neutron dose distributions in the THOR BNCT treatment room using dual TLD method," *Radiation Measurements*, vol. 43, 2008.

[91] Y. Furuta S. Tanaka, "Usage of a thermoluminescence dosimeter as a thermal neutron detector with high sensitivity," *Nucl. Instr. and Methods*, vol. 133, pp. 495-499, 1976.

[92] Application of a Bonner sphere spectrometer for determination of the energy spectra of neutrons generated by 1MJ plasma focus, "M. Králík et al.," *Rev. Sci. Instrum.*, vol. 81, 2010.

[93] I. Gamboa-de Buen, J.J.E. Herrera-Velázquez F. Castillo-Mejía, "Neutron emission characterisation at the FN-II Dense Plasma Focus," *Journal of Physics: Conference Series*, vol. 511, 2014.

[94] C. Gourlan, G. Luzzi, L. Papagno, F. Pecorella, J. P. Rager, B. V. Robouch, and M. Samuelli Ch. Maisonnier, "Plasma physics and controlled nuclear fusion research," in *Proceedings of the 4th Conference on Plasma Physics and Controlled Nuclear Fusion Research, International Atomic Energy Agency*, vol. 1, Vienna, 1971.

[95] S. Jednorog K. Szewczak, "Radiation hazards in PF-1000 plasma generator fusion research (part 3)2016," *J Radioanal Nucl Chem*, vol. 309, 2016.

[96] M.H.F. Wilkins J.T. Randall, "Phosphorescence and Electron Traps," *Proc. Roy. Soc. A*, vol. 184, no. 999, 1984.

[97] A.F. Gibson G.F.J. Garlick, "The electron trap mechanism of luminescence in sulphide and silicate phosphors," *Proceedings of the Physical Society*, vol. 60, no. 6, p. 547, 1948.

[98] A.J.J. Bos, "Theory of thermoluminescence," *Radiation Measurements*, vol. 41, no. 1, pp. S45-S56, 2006.

[99] Ma CM, "AAPM protocol for 40-300 kV x-ray beam dosimetry in radiotherapy and radiobiology.," *Med Phys.*, vol. 28, no. 6, pp. 868-893, 2001.

[100] A. Gentilini, "Comparison of four calibration techniques of a silveractivated Geiger counter for the determination of theneutron yield on the Frascati plasma focus experiment," *Nucl. Instrum. Methods*, vol. 172, 1980.

[101] F Torkzadeh and F Manouchehri, "Thermal neutron fluence measurement in a research reactor using thermoluminescence dosimeter TLD-600," *J. Radiol. Prot.*, vol. 97, no. 103, 2006.

[102] J.R. Smith, "Operation of a plasma focus device as a compact electron accelerator," *Phys. Fluids*, vol. 28, no. 7, 1985.